

Pontificia Universidad Católica del Perú
Escuela de Posgrado

Contribution to artificial tactile sensors for object contour
recognition using coupled technical vibrissae

Thesis to achieve the Degree of: Master of
Science (M. Sc.) In Mechatronics

Presented by: Stefan Eckhardt
Born am: 23.06.1992
Transit: Mechatronik
Matriculation number: 52084

Responsible Professor (TU Ilmenau): Univ.-Prof. Dr.-Ing. habil. Klaus Zimmermann
Responsible Professor (PUCP Lima): Prof. Dr. Jorge Hernan Alencastre Miranda
Supervisor (TU Ilmenau / PUCP Lima): M.Sc. Moritz Scharff

Registered on: 01.11.2019

Conceptual Formulation of the Master Thesis

of Mr. Stefan Eckhardt, BSc.

Topic: Contribution to artificial tactile sensors for object contour recognition using coupled technical vibrissae

The master thesis complements the current research activities at the Group of Biomechatronics and Technical Mechanics Group of the Technische Universität Ilmenau, as well as the activities of the Section of Mechanical Engineering of the Pontifical Catholic University of Peru. The focus is on non-visual characterization of objects using tactile sensors, which are inspired by animal vibrissae. The aim is to develop models of technical sensors which are used to determine the contact with an object, to reconstruct the boundaries/the contour of the obstacle, and to possibly detect the surface texture while scanning the surface. Current works in literature analyze the vibrissal system under various aspects and include details of the natural example like conicity. But these analyses are limited to a single hair shaft and neglected the interaction between multiple hair shafts in consequence of the elastic coupling by skin and muscles. The aim of the work is to analyze the interaction between two elastically coupled vibrissae while scanning an object for potential application as artificial tactile sensor array. Tasks of the master thesis are:

- to become acquainted with the theory presented in [Steigenberger 2013] and the corresponding literature of object scanning;
- to set up a Matlab-program for numerical simulations;
- to perform parameter studies, e.g. in dependence on the coupling stiffness;
- to model different ways to couple to hair shafts, e.g. by linear or torsional springs;
- in addition: incorporate pre-curvature, conicity of the bending rod, maybe a varying modulus of elasticity.

The master thesis shall be designed using LaTeX, all necessary files (LaTeX files, Matlab files, figures, pictures, drawings, literature files, ...) have to be put on a supplementing CD.

Date of issue: 01.11.2019
Responsible Professor (TU Ilmenau): Univ.-Prof. Dr.-Ing. habil. Klaus Zimmermann
Responsible Professor (PUCP Lima): Prof. Dr. Jorge Hernan Alencastre Miranda
Supervisor (TU Ilmenau / PUCP Lima): M.Sc. Moritz Scharff

Ilmenau, 9.10.19

Location, Date

K. Zimmermann

Signature of the responsible professor TU Ilmenau

Lima, 22 September 2019

Location, Date

J. Alencastre

Signature of the responsible professor PUCP Lima

Ilmenau 16.10.19

Location, Date

S. Eckhardt

Signature of the student

Declaration

I certify that I have independently written the work presented by me. I have marked all passages that are taken literally or in essence from published or unpublished works by others as taken. All sources and aids that I have used for the work are indicated. The work has not yet been submitted to any other examination authority with the same content or in essential parts.

The following listed persons were - in the mentioned manner - involved in the compilation, selection and implementation and evaluation of material and experiments in this work:

- The experimental verification was done in cooperation with my fellow student (B.Sc. Sebastian Müller).

No other persons were involved in the substantial development of this thesis.

Ilmenau, 20. Mai 2020

Stefan Eckhardt

Kurzfassung

Einige Säugetiere verfügen zur taktilen Umgebungserkundung über spezielle Tasthaare, die sog. Vibrissen. Die Verwendung dieses komplexen Sinnesorgans ermöglicht es bspw. Ratten Abstände und Orientierungen von Objekten sowie deren Konturen und Oberflächenbeschaffenheiten auf Basis weniger Berührungen durch ihre Vibrissen zu detektieren. Vibrissen kommen meist in Gruppen an verschiedensten Körperstellen (z.B. im Gesichtsfeld oder den Extremitäten) der Tiere vor. In der Literatur beschränken sich die meisten mechanischen Vibrissenmodelle auf die Betrachtung einer einzelnen Vibrisse, die zumeist als eingespannter Biegebalken modelliert wird. An dieser Stelle setzt die vorliegende Arbeit an und leistet einen Beitrag zur Untersuchung realitätsgetreuerer, elastisch gekoppelter Vibrissensysteme. Der Fokus liegt auf der Objektkonturabtastung und der theoretischen Erzeugung der Lagerreaktionen jeder einzelnen Vibrisse. Dabei werden das elastische Gewebe der Tiere, in das die Vibrissen eingebettet sind und die dadurch gegebene mechanische Beeinflussung der Vibrissen untereinander berücksichtigt. Zunächst erfolgt die Modellierung einer einzelnen Vibrisse durch einen langen, schlanken Balken zylindrischer Form dessen Verformungen mithilfe der nicht-linearen Euler-Bernoulli Theorie beschrieben werden. Das Modell wird anschließend in verschiedenen Abstraktionsstufen zunächst um eine elastische Lagerung und anschließend um eine zweiten Vibrisse erweitert. Die Kopplung der Vibrissen wird durch verschiedene Federstrukturen realisiert. Für die Objektabtastung wird das Vibrissenmodell quasi-statisch und translatorisch an einer exemplarisch betrachteten, streng konvexen Objekt-Profilkontur vorbeigezogen. Während der Abtastung wird zwischen den Kontaktphasen des Spitzen- und Tangentialkontakts unterschieden. Darüber hinaus werden für den Fall der Objektabtastung mithilfe mehrerer Vibrissen verschiedene Szenarien abgeleitet, um zu berücksichtigen, welche und wie viele der Vibrissen sich gleichzeitig in Kontakt mit dem Objekt befinden. Basierend auf dieser Einteilung werden verschiedene Gleichungen zur Ermittlung der Fußpunktpositionen aller Vibrissen hergeleitet. Das mechanische Modell dient als Grundlage für die Durchführung von Parameterstudien, in denen der Einfluss der Lager- bzw. Kopplungselastizität sowie des Objektabstandes auf die Lagerreaktionen der einzelnen Vibrissen untersucht wird. Dabei zeigt sich u. a., dass, im Gegensatz zum Objektabstand, eine Lagerelastizität in Abtastrichtung keinen Einfluss auf die Maximalwerte der Lagerreaktionen hat. Im Falle zweier gekoppelter Vibrissen können bestimmte Events, wie das Ablösen einer Vibrisse vom Objekt, in den Lagerreaktionen der jeweils anderen Vibrisse detektiert werden.

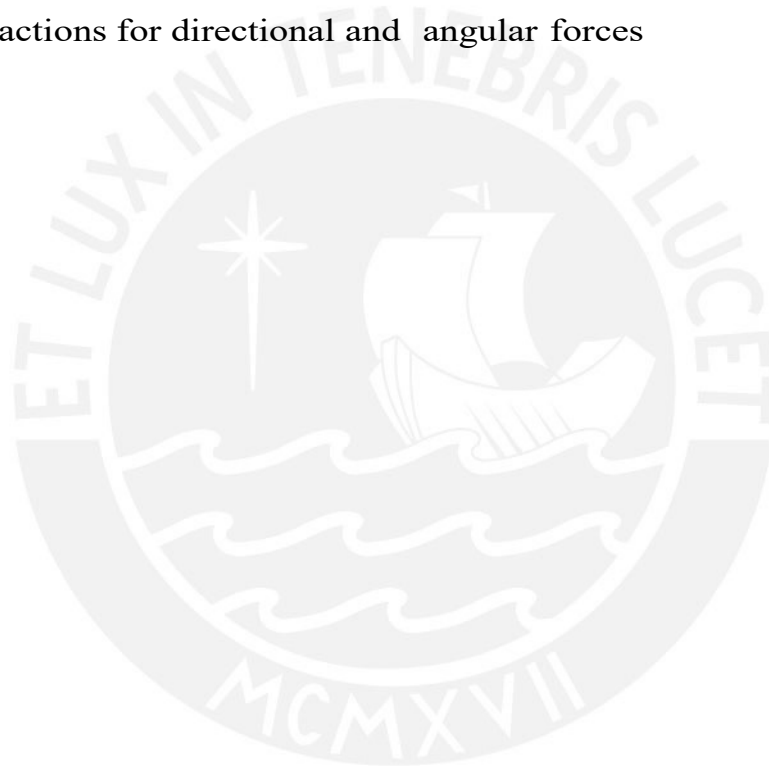
Abstract

Some mammals exhibit special tactile hairs (vibrissae) for tactile exploration of their environment. This complex sensory organ enables, e.g., rats to detect distances and orientations of objects as well as their contours and surface textures. Vibrissae are located in groups at various parts of the animal's body, e.g., in the snout region or at the extremities. In literature, most mechanical vibrissa models are limited to the consideration of a single vibrissa, usually modelled as a clamped bending beam. The present work contributes to the investigation of more realistic vibrissae systems, which are elastically coupled. The focus is on object contour scanning and a theoretical generation of the support reactions of each vibrissa. In doing so, a mutual influence of the vibrissae is taken into account. Firstly, a single vibrissa is modeled as a long, slender, cylindrically shaped beam, whose deformations are described using non-linear Euler-Bernoulli theory. The model is extended in different levels of abstraction. First, the model is adapted for an elastic support. Secondly, it is extended by a further vibrissa. The coupling of the vibrissae is realized by different structures of springs. For object scanning, the vibrissae model is swept along a strictly convex object profile contour quasi-statically and translationally. During the scanning process, a distinction is made between tip and tangential contacts. In addition, different scenarios are derived, respecting which and how many of the vibrissae are in contact with the object simultaneously. Based on this classification, the base positions of all vibrissae are determined during scanning. The mechanical model serves as a basis for parameter studies, which clarify the influence of the elasticities as well as the object distance on the support reactions of each individual vibrissa. The results show that, in contrast to the object distance, an elastic support, which is aligned with the scanning direction has no influence on the maximum values of the support reactions. Due to the elastic coupling, the snap-off of one vibrissa from the object, can be detected in the support reactions of both coupled vibrissae.

Contents

1	Introduction	1
2	Biological model	3
3	State of the art	8
3.1	Models of elastically coupled vibrissae	8
3.2	Mathematically described vibrissae models.....	11
3.3	Summary and criticism	12
4	Motivation / specification of the task	13
5	Modeling	15
5.1	Model assumptions.....	15
5.2	Model equations	17
5.3	Model extension: elastic mounting	19
5.3.1	Beam with upstream spring (model FB).....	19
5.3.2	Two coupled beams with upstream spring (model FBFB).....	19
5.3.3	Two beams with feedback (model FBFBR).....	20
5.4	Model equations of elastic support.....	20
5.4.1	Model equations for model FB.....	21
5.4.2	Model equations for model FBFB.....	21
5.4.3	Model equations for model FBFBR	23
5.4.4	Algorithm for object scanning	24
5.5	Verification of the simulation model.....	28
6	Results	34
6.1	Results for model FB	35
6.1.1	Variation of the spring stiffness	35
6.1.2	Variation of the object distance	38
6.1.3	Variation of the relaxed length of the spring (beam distance)	39

6.2	Results for model FBFB	41
6.2.1	Variation of the spring stiffness	45
6.2.2	Variation of the object distance	46
6.2.3	Variation of the relaxed length of the spring (beam distance)	48
6.3	Results for model FBFR	50
6.3.1	Variation of the spring stiffness	52
6.3.2	Variation of the object distance	53
6.3.3	Variation of the relaxed length of the spring (beam distance)	55
7	Conclusions and outlook	59
	Bibliography	65
A	Support reactions for directional and angular forces	69



List of symbols

Symbol	Bedeutung
E	Young's modulus
I_{ζ}	Second moment of area
L	Length of the bar
A	Sectional area of the beam
c	Spring stiffness
$g(p, q)$	Profile contour of the object
q	Object distance to coordinate origin
f	Contact force
f_x	Bearing force in x -direction
f_y	Bearing force in y -direction
m_{ζ}	Bearing torque about z -axis
s	Arc length of the beam
s_1	Contact point between beam and object
x_v	Control value for object scanning
x_{schnitt}	x -coordinate of the first contact
x_0	x -coordinate Base point of the bar
y_0	y -coordinate Base point of the bar
α	Profile parameters (slope angle)
η	y -coordinate of a profile point
κ	Curvature
ϕ	Bending angle
λ	Basic length of the spring
ξ	x -coordinate of a profile point

Introduction

In modern technology, there is a large number of different sensors that can perform a wide range of measuring tasks. These include optical sensors, force sensors, temperature sensors, pressure sensors and also tactile sensors. The latter are used, for example, in robotics, microsystems technology and production engineering. These sensors are able to detect object properties or contact events based on physical contacts between the sensor and an object [LN99].

In nature, too, there are a large number of mammals which, with the help of a special tactile sense organ, are able to explore objects and their characteristics. These are special tactile hairs (vibrissae), which are found on various parts of the animals' bodies. With these tactile hairs it is possible, for example, for rats to detect object shapes and surface properties.

Numerous research teams from different scientific disciplines are working on the synthesis of technical sensors based on the model of vibrissae. Numerous mechanical models for object scanning and reconstruction as well as prototypes of individual technical vibrissae sensors already exist. Currently, it is possible to bring vibrissae sensors into contact with an object and to obtain information about the object using the measured support reactions. However, this work is often limited to the observation of a single isolated hair. Vibrissae, however, occur mainly in the facial area of the animals mostly in groups and are elastically supported in skin and tissue.

Inspired by the biological model, this work investigates how elastic couplings of several technical vibrissae affect the signals during object scanning. For this purpose, numerical simulations are performed with *MATLAB* using different models of vibrissae coupling. In a parameter study the influence of the elastic coupling and the object distance on the mechanical signals at the mounted end of a vibrissae sensor is investigated.

For an analysis of the biological model, the following chapter summarizes the current state of scientific knowledge about the biology of vibrissae.



Biological model

Vibrissae are a special type of hairs that occur in the animal world. They enable animals to perceive their environment tactilely and are therefore also called tactile hairs. Rats and mice can use their vibrissae to recognize object positions, orientations and properties, e.g. object contours or surface textures [Pea62],[PMG11].



Figure 2.1: Examples of vibrissae in nature: (a) mystical vibrissae of a rat [PMG11]; (b) carpal vibrissae of a rat [SWZ`14].

Vibrissae differ from hairs of the coat in their length, thickness and the depth of rooting in the surrounding tissue (see fig. 2.2). They have a conical shape and are pre-curved [QH12, HPSG13, TQG`11, IW75]. The term vibrissa only refers to the passive part (outer hair shaft) of the sensory organ. The hair shaft, hair follicles and the surrounding tissue, which represent the entire sensory organ, can be summarized as the follicle-sinus-complex (FSC) [Kla99, EKM`02, FPR97]. An FSC always consists of a venous blood sinus, which is placed under the skin around a hair follicle. The blood sinus consists of different chambers which are filled with blood. In [Car09, Dö82, FPR97] the hypothesis was put forward that by means of the adjustable blood pressure the filling volume of the blood sinus and thus the stiffness and damping properties of the tactile hair bearing can be regulated.

The actual hair has no receptors along the hair shaft. Therefore, the forces and moments resulting from contact with the object must be mechanically transmitted to the nerves. These nerves are located around the hair root and convert the forces and moments into electrical signals, which are then transmitted to the animal's nervous system [Kre10, EKM`02, QH12].

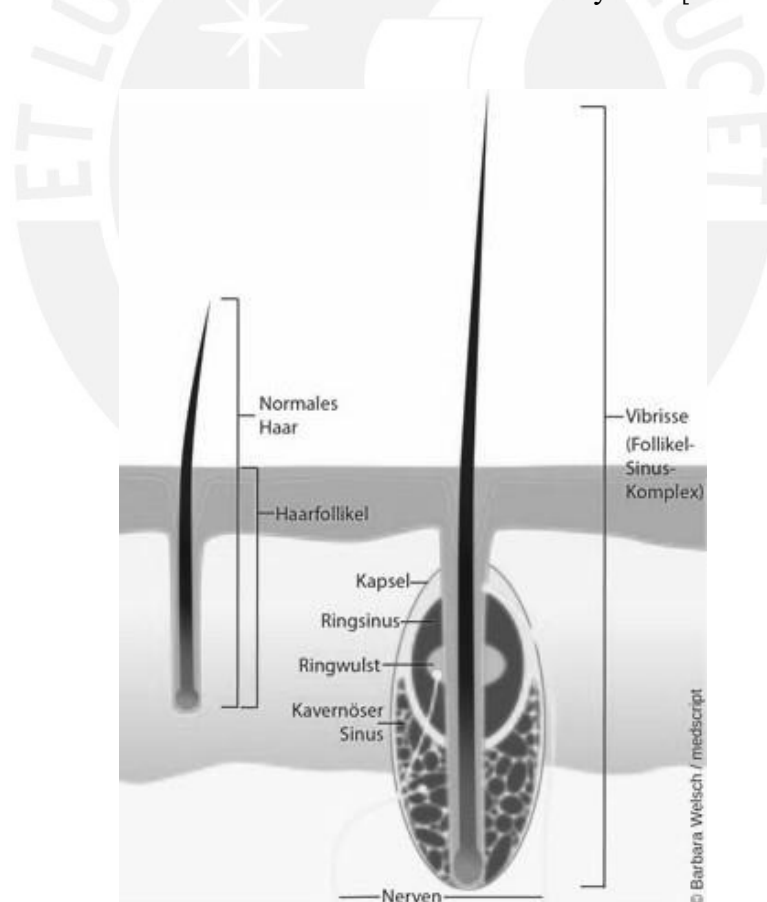


Figure 2.2: Comparison of the structure of a vibrissae with that of a normal hair [Wel18].

Each FSC is covered by a muscle loop in the blood sinus area (see figure 2.3). Through this it is possible to control each individual vibrissa and initiate a movement [Car09]. This results in two operating modes [CK06, Car09]:

- **Active Mode:** During active palpation, the vibrissa are set in motion by the muscles. The frequency of the oscillation is between 2 Hz and 20 Hz with an amplitude of 31.6 μ m to 56.2 μ m. In this mode, contours and surface properties can be examined more closely [Car09, MGA¹¹].
- **Passive Mode:** During passive scanning, the vibrissa is not actively vibrated. Only external forces lead to a deflection of the vibrissa [Car09].

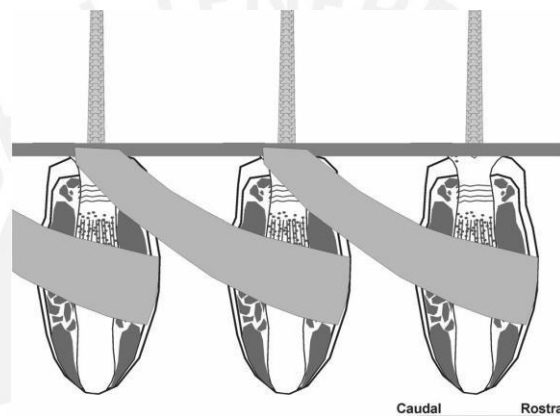


Figure 2.3: Muscle loop [Car09].

These scanning strategies help the animals to accomplish the following tasks:

- **Localization:** Localization is used to detect objects and gaps. Thereby, the object location, the intensity of the contact, the time of deflection and the relative position of the object to the head is detected [AK11].
- **Shaped distinction:** Rats are capable of identifying macroscopic features by active or passive probing [PMG11, TSJH12].
- **Texture discrimination:** Based on vibrations when scanning a surface, texture differences can be identified [PMG11, AHD09].
- **Tracing:** In addition to other sensory organs, vibrissae are used to detect prey [Ahl05].
- **Orientation:** Some animals use their vibrissae to maintain their body position in the water or to obtain information about the position of the nostrils on the water surface [Ahl05].

Arrangement of vibrissae

Vibrissae can be found at various points of the head and extremities. Most of them are found in the head area in defined fields in the area of the eyes and the mouth and nose openings (see fig. 2.4). The tactile hairs around the muzzle of the animal (mystacial vibrissae) are the most conspicuous and are considered the most important group. They are often referred to as primary vibrissae [BPM97].

The tactile hairs on the extremities which are available for locomotion are called carpal vibrissae [Kla99].

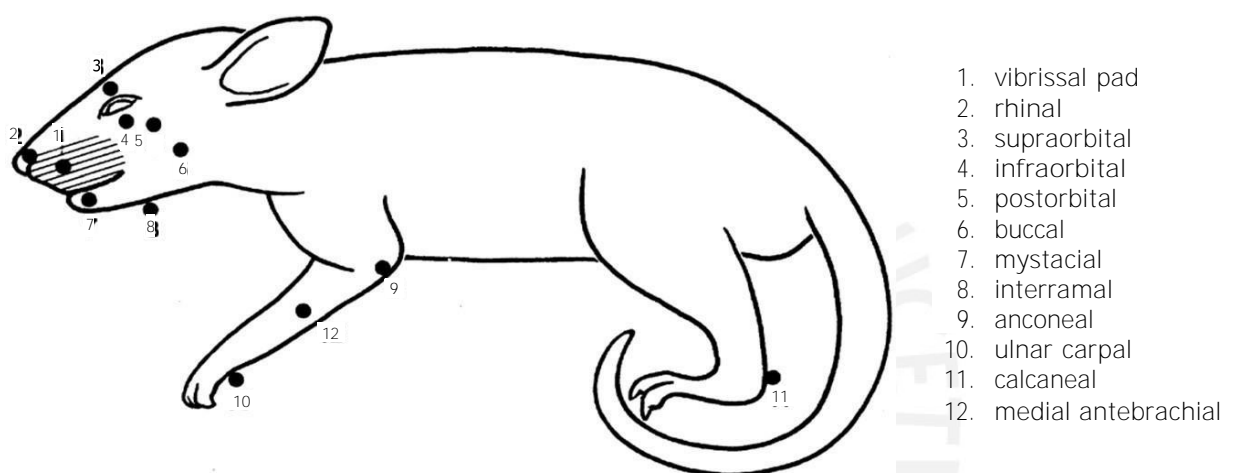


Figure 2.4: Vibrissae distribution of a rat [Kla99].

In order to achieve an easier classification of the individual mystacial vibrissae, the following nomenclature has become established: The five rows are designated from dorsal to ventral with the letters A to E. The individual vibrissae are numbered from occipital to rostral. Furthermore, there are four vibrissae at the edge of this field, which are larger than the rest. These are designated with the Greek letters α , β , γ and δ (see fig. 2.5) [Kla99, BPM97].

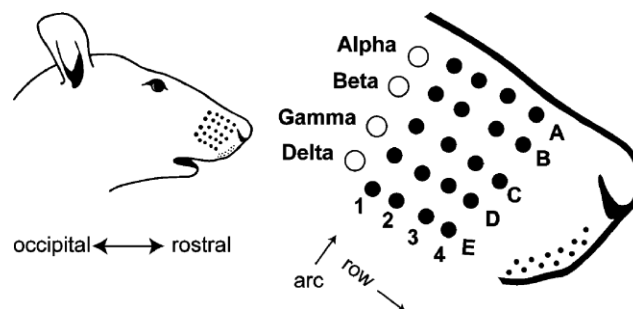


Figure 2.5: Mystacial vibrissae of a rat [VCK¹²].

Carpal vibrissae are mainly found in mammals that live in trees. But also rats possess this type of tactile hair on the distal end of the forearm in small groups of three hairs. In contrast to the mystacial vibrissae, these cannot be actively moved according to the current state of research [HVN¹⁴].

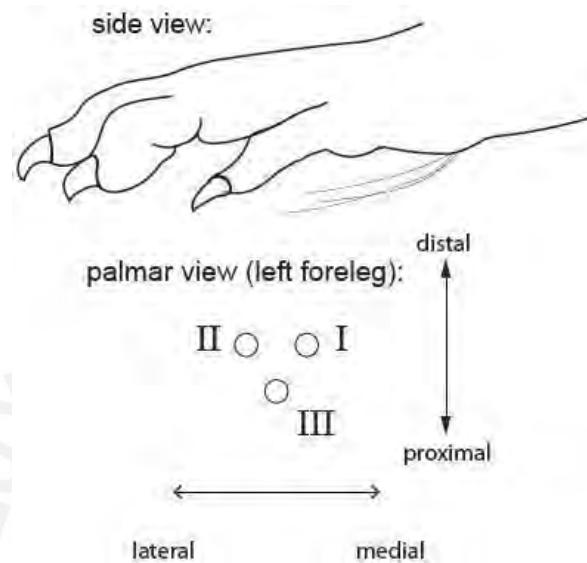


Figure 2.6: Carpal vibrissae of a rat [HVN¹⁴].

In the context of the present work the coupling of mystacial vibrissae is treated. Therefore, a closer examination of other types of vibrissae will be omitted.

In summary, important features of biology should be recorded, which are taken into account in the modelling within the scope of this work:

- Vibrissae are long, slender elastic hairs - and have a conical and pre-curved shape, which is not considered below [QH12].
- Vibrissae are flexible, elastic feelers that have no receptors and act as stimulus transmitters [Kla99, WK10].
- Vibrissae are resiliently mounted in the follicle-sinus complex. That is also where the mechanoreceptors are located [Kla99].
- It is hypothesized that the elastic support is adjustable by blood pressure changes of the follicle-sinus complex [Car09].
- Vibrissae occur mostly in groups with small intervals [Kla99].
- Vibrissae are used for object scanning by passive palpation or active scanning by activating the muscles [Car09].

State of the art

With regard to the objective of the present work, the following consideration of the state of the art focuses on such models which consider an elastic coupling of several vibrissae.

3.1 Models of elastically coupled vibrissae

In the literature, there are various approaches to reproduce the elastic support of a vibrissa in the skin and tissue. The biological model is reproduced at different approximation levels.

In the simplest case, the elasticity is simulated by a single horizontal or vertical translation spring or a single torsion spring (see fig. 3.1) [MBSZ19, WBS17].

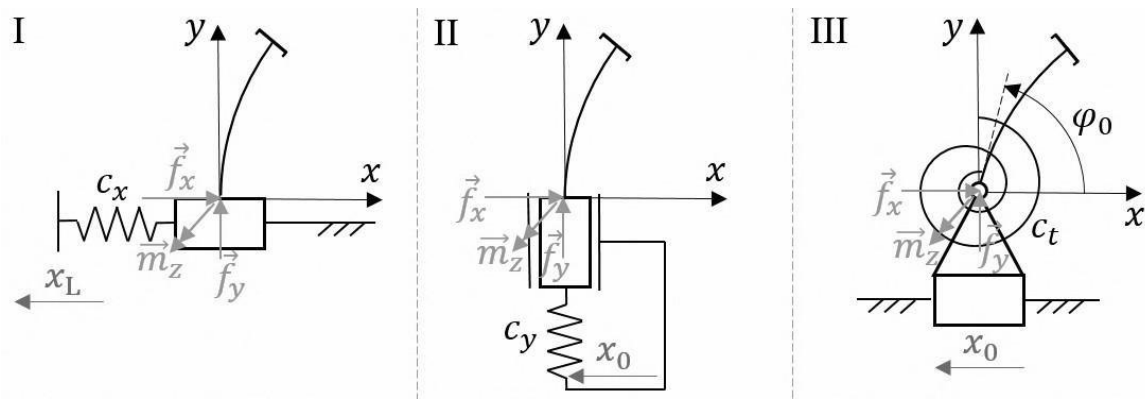


Figure 3.1: Vibrissae model according to Merker [MBSZ19].

More realistic approaches, on the other hand, use several springs to replicate the elasticity of the skin tissue.

A first variant is shown in fig. 3.2. Both the skin and the tissue are modeled as springs. These are horizontally oriented; a simulation of the elasticity in vertical direction or a torsional stiffness is not implemented. Furthermore, the musculature for active palpation is shown [BK03].

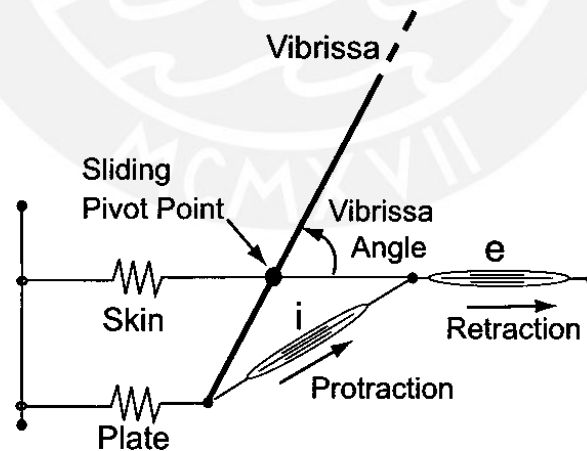


Figure 3.2: Vibrissae model according to Berg [BK03].

Another model from the literature (see fig. 3.3) also maps an elasticity in vertical direction. Furthermore, the equivalent circuit also has damping elements which influence the dynamics of the system [SBH⁺10].

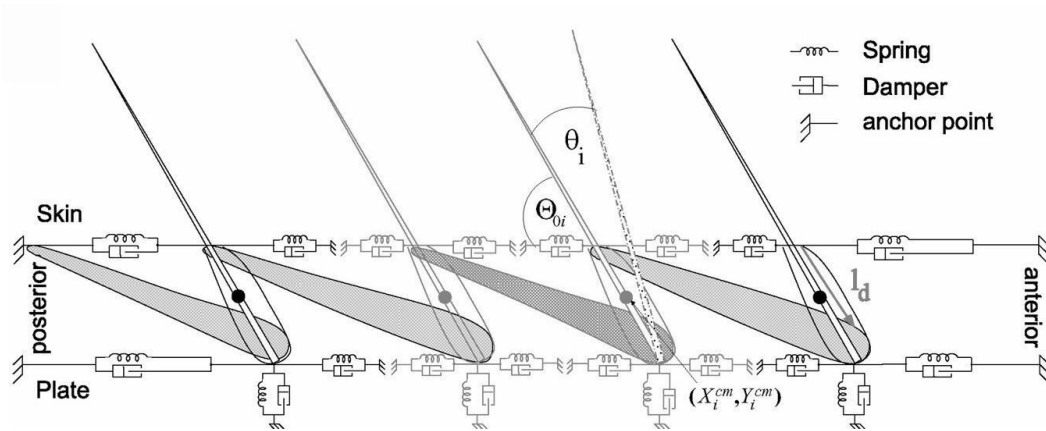


Figure 3.3: Vibrissae model according to Simony [SBH`10].

In nature, however, it is not only the skin and surrounding tissue that have elastic properties, but also the FSCs themselves. The elasticity of the FSC is described in the model of [SSWB11] (see fig. 3.4) is taken into account. The black frame shows the components of the FSC. The hypothesis of adjustable blood pressure in the blood sinus is taken into account in the form of adjustable damper and spring elements. Furthermore, the elastic effect of the muscles as well as that of the skin and tissue is simulated [SSWB11].

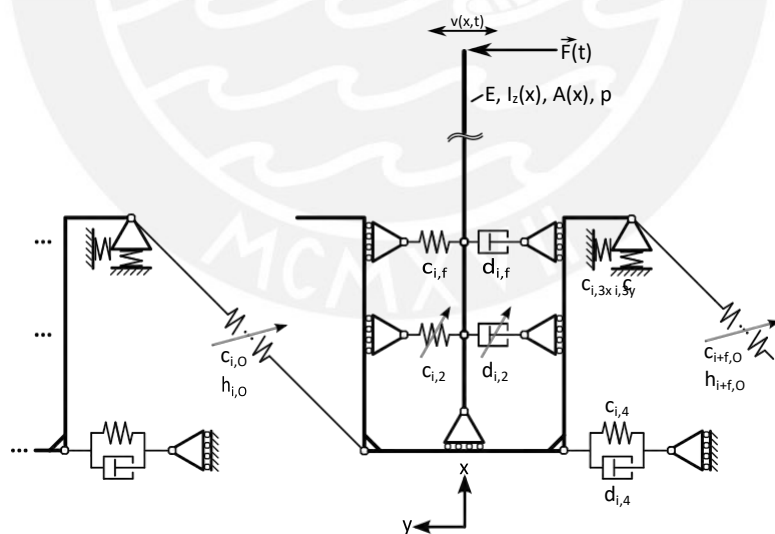


Figure 3.4: Vibrissae model according to Schäfer [SSWB11].

Although these models are partly detailed reproductions of the biological model, they are not described mathematically for the most part and therefore serve mostly as illustrations. Nevertheless, there are also models that are described mathematically and take into account large vibrissae deformations. These will be briefly summarized below, with the focus on

preliminary work at the Department of Technical Mechanics at the Technical University of Ilmenau.

3.2 Mathematically described vibrissae models

A model for the continuous scanning of strictly convex object contours is shown in [WBS17]. A single vibrissae is translated along the object (see fig. 3.5). The calculation of the deformation states and the support reactions is carried out by solving a two-point boundary value problem. In the second step it is possible to use the determined support reactions by solving an initial value problem for the reconstruction of a sequence of contact points [WBS17].

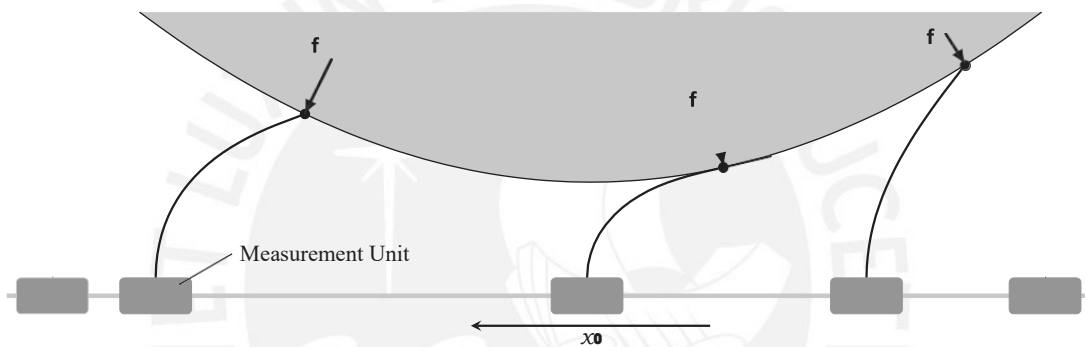


Figure 3.5: Translational scanning of a strictly convex object contour [WBS17].

In [Mer17] this model was extended by a rotational movement of the vibrissae by adjusting the boundary conditions. In both publications, based on [Ste13], a distinction was made between tip contact and tangential contact when formulating the boundary conditions with regard to the type of contact. Among other things, the effect of the object distance on the simulated support reactions was investigated.

The work presented is limited to flat models. In [CR06], however, a model is presented which allows the reconstruction of three-dimensional objects. As in the previously mentioned works, contact localization is achieved by numerical integration of the deformation equations. The bending moment in the artificial vibrissa at the point of contact is used to make use of the fact that the bending moment disappears.

3.3 Summary and criticism

In the literature there are different models for the simulation of elastic vibrissae support and coupling. These range from very simple models to very extensive, more realistic models. While such models, which are limited to the observation of a single vibrissa, are often described mathematically, model equations for elastically coupled vibrissae systems are rarely found. A simulative investigation of such and the theoretical calculation of the support reactions of elastically coupled vibrissae during object scanning could not be found in an analysis of the state of research.

The mathematical model of [Ste13] is suitable for object scanning. It takes into account both large deformations of the beam and a differentiation of the contact between beam and object in point and tangential contact. Furthermore, the model is completely analytically describable and has already been extensively validated by experiments [MSZB18, MFS`20]. First extensions of the mentioned model by an elastic support already exist [MBSZ19, WBS17]. The simulation results obtained in this context can be used for comparison purposes with the results of the present work. For the reasons mentioned above, the existing mathematical model from [Ste13] is extended in the context of this thesis to include translational object scanning for the elastic coupling of adjacent vibrissae.

Motivation / specification of the task

Within the framework of the present work, a beam model with elastic support between individual beams is to be developed and investigated. In previous preliminary work of the research group of the TU Ilmenau and the PUCP, the scanning of an object contour by means of a beam is done translatory or rotatory. In the animal kingdom, however, vibrissae usually occur in groups and are elastically coupled with each other by the surrounding tissue and skin. This is the starting point of the present work. Based on the natural model of the vibrissae, the interaction of neighbouring tactile hairs shall be modelled and the influences of different parameters of the elastic coupling on the support reactions during scanning shall be clarified. For this purpose the following main topics are treated:

- Extension of the existing model of a translational beam movement [Ste13] considering elastic influences of the FSC and the surrounding tissue.
- Description of beam deformation using non-linear Euler-Bernoulli bending theory.
- Transfer of the biological model into a mechanical model with different levels of abstraction.
- Development of a Matlab algorithm for object scanning of a strictly convex profile and theoretical generation of the support reactions.

- Numerical investigation of the influence of bearing elasticity and object distance on the deformations and the associated support reactions.



Modeling

The aim of this chapter is the development of mechanical models for profile scanning using elastically coupled vibrissae.

5.1 Model assumptions

The model used in this thesis (in fig. 5.1) is based on [Ste13]. It consists of an artificial vibrissa in contact with an object. In the following, model assumptions from [Ste13] are summarized and extended:

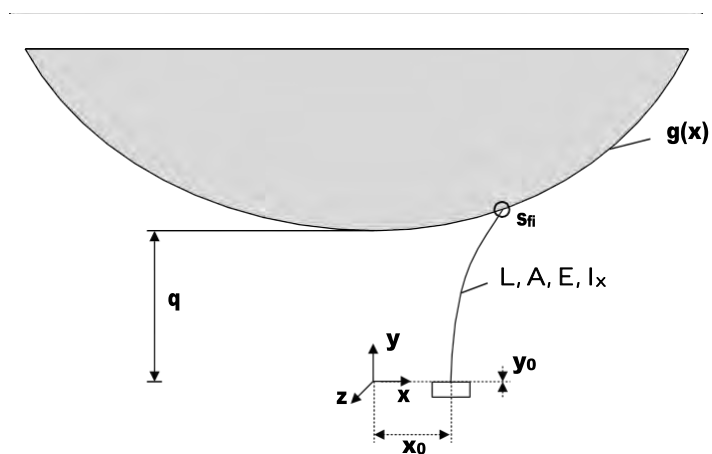


Figure 5.1: Artificial vibrissa in contact with an object.

1. Artificial vibrissa

- The artificial vibrissa is modeled as a bending beam with the length L .
- The material has a constant modulus of elasticity E .
- The cross-section A of the beam and thus the corresponding equatorial moment of inertia is constant.
- The beam is vertically clamped or elastically supported at the lower end.
- In the unloaded state, the beam is straight.

2. Object

- The object must be regarded as a rigid body.
- The profile contour $g(x)$ of the object is strictly convex and parameterized as a function of the slope angle α of the contour.
- The vertex of the object has a y distance q to the coordinate origin, the x coordinate lies at the coordinate origin.

3. Contact

- Due to the strictly convex profile contour of the object, there is only one contact point between beam and object at any given time.
- Furthermore, friction effects between object and beam are neglected. Therefore the contact force is always perpendicular to the profile tangent of the object.

4. Scanning method

- The scanning takes place in one plane (plane problem).
- The scanning is realized by moving the clamping (base x_0) of the artificial vibrissa stepwise in negative x direction (kinematic drive).
- The movement is performed very slowly. Therefore, the scanning process can be regarded as quasi-static.
- The deformation states are calculated using the non-linear Euler-Bernoulli theory.

5.2 Model equations

In order to allow arbitrary scaling, the following units of measurement are introduced to derive the model equations following [Ste13]:

$$\begin{aligned}
 \text{rLengthss} &: " \frac{L}{EI_z} \\
 \text{rForcess} &: " \frac{L^2 EI_z}{EI_z} \\
 \text{rMomentss} &: " \frac{L}{EI_z} \\
 \text{rSpring stiffnesss} &: " \frac{EI_z}{L^3}
 \end{aligned} \tag{5.1}$$

Taking into account the assumptions described in section 5.1, the system of differential equations can be used to calculate the deformation of the beam as a function of the force f , the angle $\alpha \in \left[-\frac{\pi}{2}, \frac{\pi}{2}\right]$ and the position of the contact point $s_1 \in [0, L]$ (5.2) [Ste13].

$$\begin{aligned}
 x'(s) &= \cos\phi(s) \\
 y'(s) &= \sin\phi(s) \\
 \phi'(s) &= \kappa(s) \\
 \kappa'(s) &= -\frac{f}{EI_z} \cos\phi(s) - \alpha \delta(s - s_1)
 \end{aligned} \tag{5.2}$$

During object scanning, a distinction must be made between two types of contact:

1. Top contact (phase A)

The contact point is located at the top of the beam ($s_1 = 1$). The contact angle is unknown ($\phi(1) \neq \alpha$). The following boundary conditions result for the tip contact [Ste13]:

$$\begin{aligned}
 x(1) &= \xi_{\text{ra}} \\
 y(1) &= \eta_{\text{ra}} \\
 \kappa(1) &= 0
 \end{aligned} \tag{5.3}$$

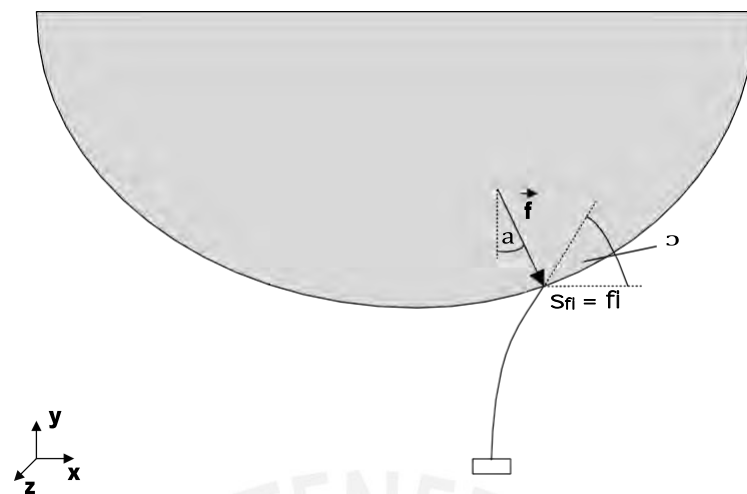


Figure 5.2: Deformed beam on tip contact.

2. Tangential Contact (Phase B)

With tangential contact, the position of the contact point s_1 along the rod axis is unknown. The following boundary conditions result for tangential contact [Ste13]:

$$\begin{aligned}
 x_{p_{s_1}} &= \xi_{p_{a_1}} \\
 y_{p_{s_1}} &= \eta_{p_{a_1}} \\
 \phi_{p_{s_1}} &= \alpha \\
 \kappa_{p_{s_1}} &= 0
 \end{aligned}
 \tag{5.4}$$

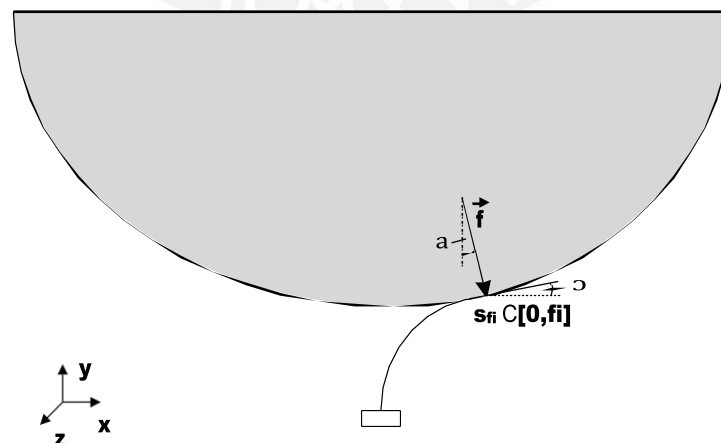


Figure 5.3: Deformed beam on tangential contact.

5.3 Model extension: elastic mounting

In order to take the elasticity of the FSC into account, the model presented below is extended by an elastic mounting. For this purpose, different levels of abstraction are modelled.

5.3.1 Beam with upstream spring (model FB)

In the first level of abstraction, the mechanical model from section 5.2 is extended by an upstream spring (see fig. 5.4). This model will be referred to below as model FB (spring-beam). In this case, the position is not specified at the base x_0 during scanning, but by specifying the manipulated variable x_v . The spring has a spring stiffness c_1 and a basic length λ_1 .

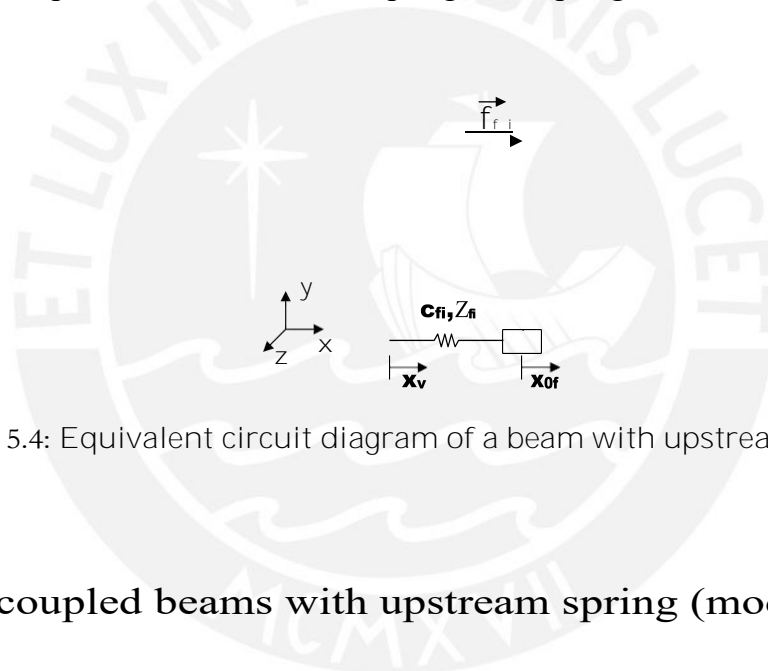


Figure 5.4: Equivalent circuit diagram of a beam with upstream spring.

5.3.2 Two coupled beams with upstream spring (model FBFB)

In the next step, the model is to be extended by a further beam (at a distance of λ_2) (see fig. 5.5). The two beams are coupled by a spring of stiffness c_2 . Furthermore, the position is determined by the manipulated variable x_v on the upstream spring. The model is called model FBFB (spring-beam-spring-beam).

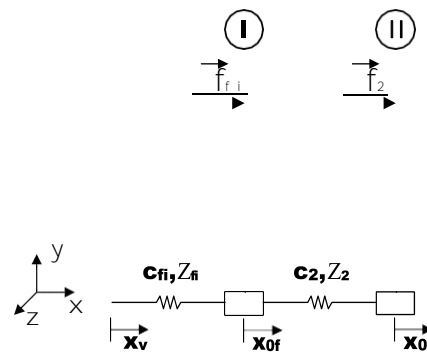


Figure 5.5: Equivalent circuit diagram of two coupled beams with upstream spring.

5.3.3 Two beams with feedback (model FBFBR)

In biology, however, the vibrissae are not only elastically coupled with each other, but are also embedded in the elastic tissue of the skin. In order to take this into account, the model has been extended by an additional spring (feedback) (see fig. 5.6). This connects the base point of the second beam x_{02} with the tension point (manipulated variable) x_v , where the displacement is specified. As with the previous models, this will be referred to below as model FBFBR (spring-beam spring-beam feedback).

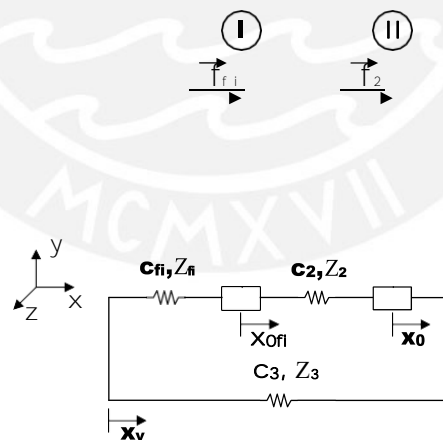


Figure 5.6: Equivalent circuit diagram of two beams with coupling to the frame.

5.4 Model equations of elastic support

To implement the approaches worked out in section 5.3 in *MATLAB*, the corresponding model equations are derived below.

5.4.1 Model equations for model FB

For the model equation of a beam with upstream spring (see section 5.3.1) the forces are cut free and then the equilibrium of forces is established:

$$f_1 \sin \alpha_1 q - c_1 p x_{01} - x_{01} q = 0 \quad (5.5)$$

Changing the equation returns the base point position x_{01}

$$x_{01} = \frac{f_1 \sin \alpha_1 q}{c_1} - x_{01} q \quad (5.6)$$

To consider the basic length of the spring, it must be added below:

$$x_{01_{abs}} = x_{01} + \lambda_1 \quad (5.7)$$

5.4.2 Model equations for model FBFB

When simulating several coupled beams, different contact scenarios can occur. Here it must be distinguished how many and which beams are in contact with the object at the same time (subsequently assigned accordingly with the variable *Flag Phase*). Depending on the contact scenario, the switching of the springs and thus the equations for calculating the foot points of the beams change.

In the following, the model equations for two coupled beams with an upstream spring (see section 5.3.2) are established by establishing equilibria of forces for the general case (both beams are in contact, *Flag Phase* = 2) and then deriving the individual contact scenarios as special cases.

Balance of forces for beams 1:

$$f_1 \sin \alpha_1 q - c_1 p x_{01} - x_{01} q - c_2 p x_{01} - x_{02} q = 0 \quad (5.8)$$

Balance of forces for beams 2:

$$f_2 \sin \alpha_2 q - c_2 p x_{02} - x_{01} q = 0 \quad (5.9)$$

After converting the equations (5.8) and (5.9) to x_{02} as well as equating, the following relationship is obtained for x_{01}

$$x_{01} = \frac{f_1 \sin \alpha_1 q}{c_1} - \frac{f_2 \sin \alpha_2 q}{c_1} - x \quad (5.10)$$

For the absolute position $x_{01, abs}$ the basic spring length λ_1 must be added:

$$x_{01, abs} = x_{01} + \lambda_1 \quad (5.11)$$

The converted formula (5.9) can be used for the position calculation of the base point of beam 2:

$$x_{02} = \frac{f_1 \sin \alpha_1 q}{c_1} - \frac{f_2 \sin \alpha_2 q}{c_1} - \frac{f_2 \sin \alpha_2 q}{c_2} - x \quad (5.12)$$

with associated absolute position:

$$x_{02, abs} = x_{02} + \lambda_1 + \lambda_2 \quad (5.13)$$

In the following two special cases are considered.

Only beam 1 in contact (*Flag Phase* " 1):

There is only a contact force between beam 1 and object ($f_1 \neq 0, f_2 = 0$). From (5.11) and (5.12) the following equations result for the base points:

$$x_{01, abs} = \frac{f_1 \sin \alpha_1 q}{c_1} - x + \lambda_1 \quad (5.14)$$

$$x_{02, abs} = \frac{f_1 \sin \alpha_1 q}{c_1} - x + \lambda_1 + \lambda_2$$

Only beam 2 in contact (*Flag Phase* " 3):

There is only a contact force between beam 2 and object ($f_1 = 0, f_2 \neq 0$). Thus, (5.11) and (5.12) result in the following equations for the base points:

$$x_{01, abs} = \frac{f_2 \sin \alpha_2 q}{c_1} - x + \lambda_1 \quad (5.15)$$

$$x_{02, abs} = \frac{f_2 \sin \alpha_2 q}{c_2} - \frac{f_2 \sin \alpha_2 q}{c_1} - x + \lambda_1 + \lambda_2$$

5.4.3 Model equations for model FBFBR

Analogous to section 5.4.2, a distinction of the contact scenarios must also be carried out for the model of two beams with feedback (see section 5.3.3). For this purpose, the general equations (both beams in contact, *Flag_Phase* “ 2) are derived below and then two special cases are derived:

Balance of forces for beams 1:

$$f_1 \sin \alpha_1 q - c_1 p_{x_{01}} - x_{01} q - c_2 p_{x_{01}} - x_{02} q = 0 \quad (5.16)$$

Balance of forces for beams 2:

$$f_2 \sin \alpha_2 q - c_2 p_{x_{02}} - x_{01} q - c_3 p_{x_{02}} - x_{02} q = 0 \quad (5.17)$$

Converting and equating the equation (5.16) and (5.17) after x_{02} gives the following relation for x_{01} :

$$x_{01} = \frac{f_1 \sin \alpha_1 q c_2 - c_3 q - f_2 \sin \alpha_2 q c_2}{c_1 c_2 - c_1 c_3 - c_2 c_3} \quad (5.18)$$

To determine the absolute position $x_{01, abs}$ the basic spring length λ_1 must be added again:

$$x_{01, abs} = x_{01} + \lambda_1 \quad (5.19)$$

The base point position of beam 2 can be determined by changing the formula (5.17):

$$x_{02} = \frac{f_2 \sin \alpha_2 q - c_2 x_{01} - c_3 x_{02}}{c_2 - c_3} \quad (5.20)$$

with associated absolute position:

$$x_{02, abs} = x_{02} + \lambda_1 + \lambda_2 \quad (5.21)$$

Only beam 1 in contact (*Flag Phase* "1):

There is only contact between beam 1 and object ($f_1 \neq 0, f_2 = 0$). Thus, (5.19) and (5.21) result in the following equations for the footers:

$$\begin{aligned} x_{01, abs} &= \frac{f_1 \sin \alpha_1 q c_2}{c_1 c_2 + c_1 c_3 + c_2 c_3} - x_v - \lambda_1 \end{aligned} \quad (5.22)$$

$$\begin{aligned} x_{02, abs} &= \frac{f_1 \sin \alpha_1 q c_2}{c_1 c_2 + c_1 c_3 + c_2 c_3} - x_v - \lambda_1 - \lambda_2 \end{aligned}$$

Only beam 2 in contact (*Flag Phase* "3):

There is only a contact force between beam 2 and object ($f_1 = 0, f_2 \neq 0$). This results in the following equations for the base points:

$$\begin{aligned} x_{01, abs} &= \frac{f_2 \sin \alpha_2 q c_2}{c_1 c_2 + c_1 c_3 + c_2 c_3} - x_v - \lambda_1 \\ x_{02, abs} &= \frac{f_2 \sin \alpha_2 q}{c_2 + c_3} - \frac{f_2 \sin \alpha_2 q c^2}{\rho c_1 c_2 + c_1 c_3 + c_2 c_3 q \rho c_2 + c_3 q} - x_v - \lambda_1 - \lambda_2 \end{aligned} \quad (5.23)$$

A distinction must also be made in the program flow with regard to the number of beams and the respective contact scenarios. For this purpose, an algorithm was developed in the context of this thesis, which is presented in the following.

5.4.4 Algorithm for object scanning

This simulation algorithm used (see fig. 5.9) in *MATLAB (Version R2015b)* is based on the contact scenarios described (see section 5.4.2). At the beginning the x -coordinate $x_{intersection}$ of the point is calculated at which the undeformed beam touches the object for the first time when x_v is reduced (see fig. 5.7). This intersection is used to determine the start point of the simulation and to detect whether beam 2 is in contact or not ($x_{02} \geq x_{schnitt} \wedge x_{02} \leq x_{schnitt}$). For the first contact it can be assumed that only beam 1 is in contact with the object (*Flag Phase* "1). The starting point is the base points:

$$\begin{aligned} x_{01} &:= x_{schnitt} \\ x_v &:= x_{schnitt} - \lambda_1 \end{aligned} \quad (5.24)$$

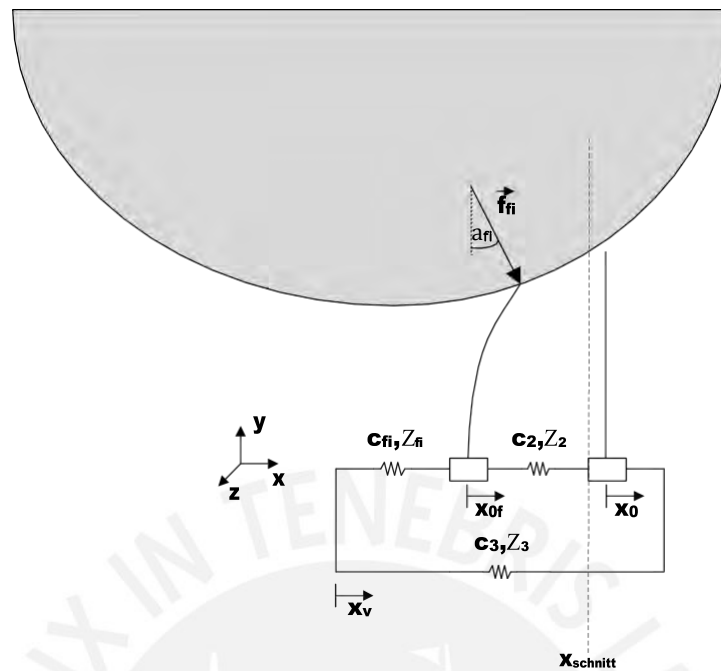


Figure 5.7: Exemplary representation of contact scenario 1 (*Flag Phase* “ 1).

The subsequent deformation calculations are carried out in a loop in which the change in the manipulated variable x_v takes place at equidistant intervals Δx_v .

For the calculation of the unknown parameters (f_i , α_i and $s_{1,i}$) of each beam the solution algorithm *fsolve* implemented in *MATLAB* is used. Here, the boundary conditions must be specified according to the type of contact (tip contact and tangential contact) (see section 5.2). The query as to which contact state exists is performed in the algorithm used as follows [Mer17]:

1. Calculation of the deformation with the assumption that phase B (tangential contact) exists.
2. Check for a contradiction ($s_1 \tilde{\neq} 1$)
 - Yes: assumption was correct (beam is tangentially in contact with the object at s_1)
 - No: contradiction (beam is in contact at $s_1 \neq 1$) $\tilde{\rightarrow}$ recalculation with equations (5.2) and (5.3) for tip contact

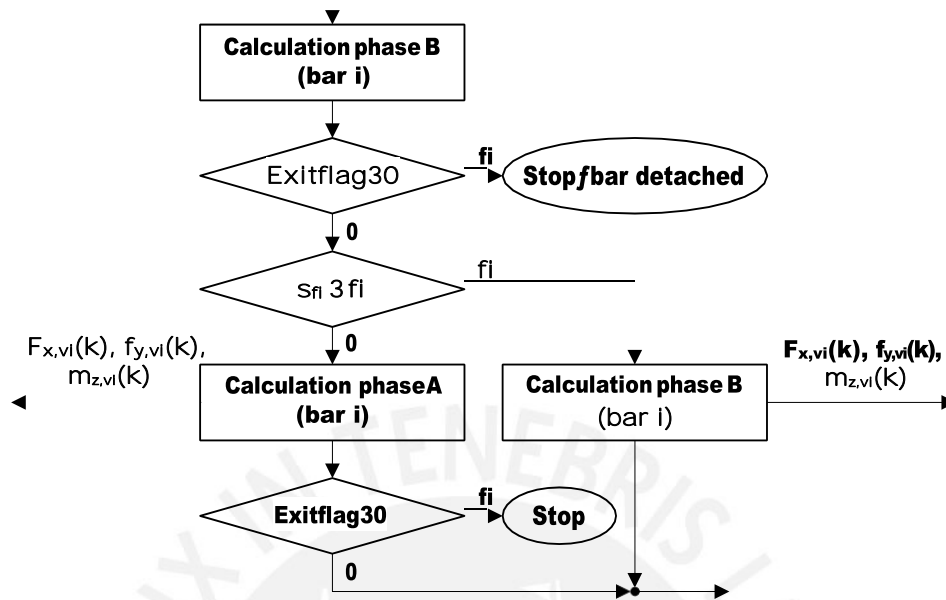


Figure 5.8: Algorithm for the deformation calculation of a vibrissa.

Afterwards it is tested which scenario was present in the previous step and accordingly the position of the foot points and the deformations of the beams are calculated. If there is a change in the contact scenario (beam 2 made contact or beam 1 jumped off), the calculation is repeated using equations from the next scenario. This calculation is performed for the same manipulated variable x_v and the variable *Flag Phase* is changed accordingly.

After each deformation calculation, the *fsolve* parameter returned by *fsolve* is used to check whether a solution has been found. If not, the program terminates with an error message (see fig. 5.9).

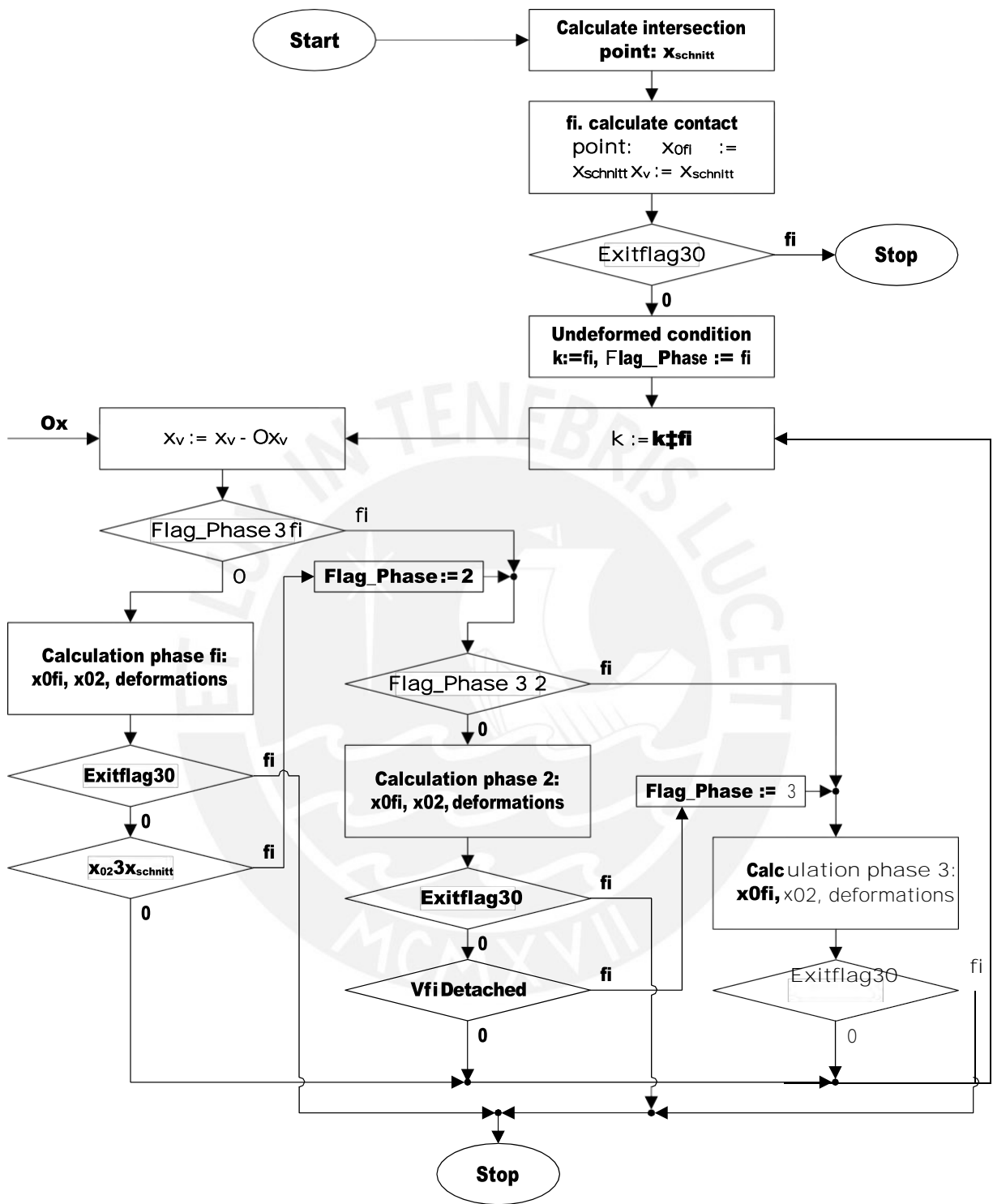


Figure 5.9: Algorithm for simulating object scanning using two beams.

5.5 Verification of the simulation model

In the following section a verification of the resulting simulation model is carried out. The results are compared with simulations of a parallel work with the title „Determination of the signals recorded by carpal vibrissae of rats during locomotion and forelimb touch down“ [Mü20].

Thereby the simulations are performed according to the method of multi-body dynamics with the program *ALASKA* (Version 9.7.2) was performed. To minimize deviations due to dynamic influences, the simulations were carried out with slow force changes or speeds.

In both operations, a single beam was first loaded with a force and then an object was scanned. In these simulations, the deformation states and the corresponding forces and moments in the clamping are calculated.

In the following, the results of several simulations are compared. Simulations with directional force¹ and carried force² is compared, considering different amounts of the de-dimensionalized force (1,3,5,7,10) and different force introduction points (30%, 50%, 70% and 100% of the beam).

The deformation of the beam is calculated using *ALASKA* in discrete points. These are represented in the following graphics by red crosses. The results are visualized as a solid blue line using *MATLAB*.

In fig. 5.10 the deformations of a beam are shown with a variation of the amounts of the force carried. In fig. 5.11 the point of force application varies along the vibrissa.

Qualitatively, the deformation is plausible in both cases. Also the overlapping of the deformation in fig. 5.10 at 10 N can be explained by the fact that the y-component of the force is small in terms of amount. At lower forces, this component is larger and leads to a stronger shift in the y-direction.

¹is a force that does not change the direction of action when the point of application of the force is shifted [GHSW17]

²is a force, which maintains the relative angle to the beam in each deformation state [GHSW17]

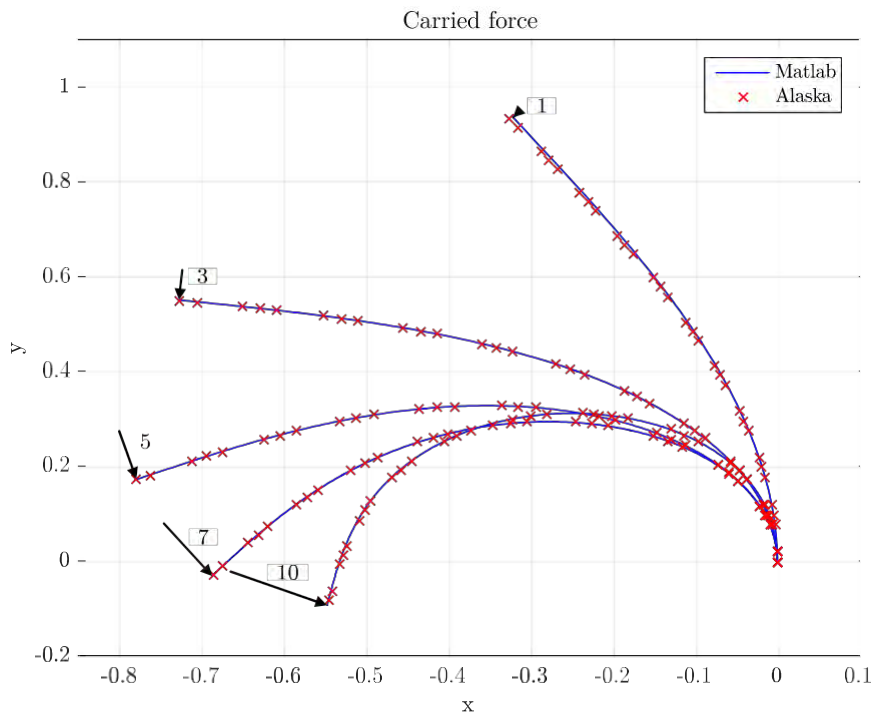


Figure 5.10: Deformation with entrained force at varied force amplitude.

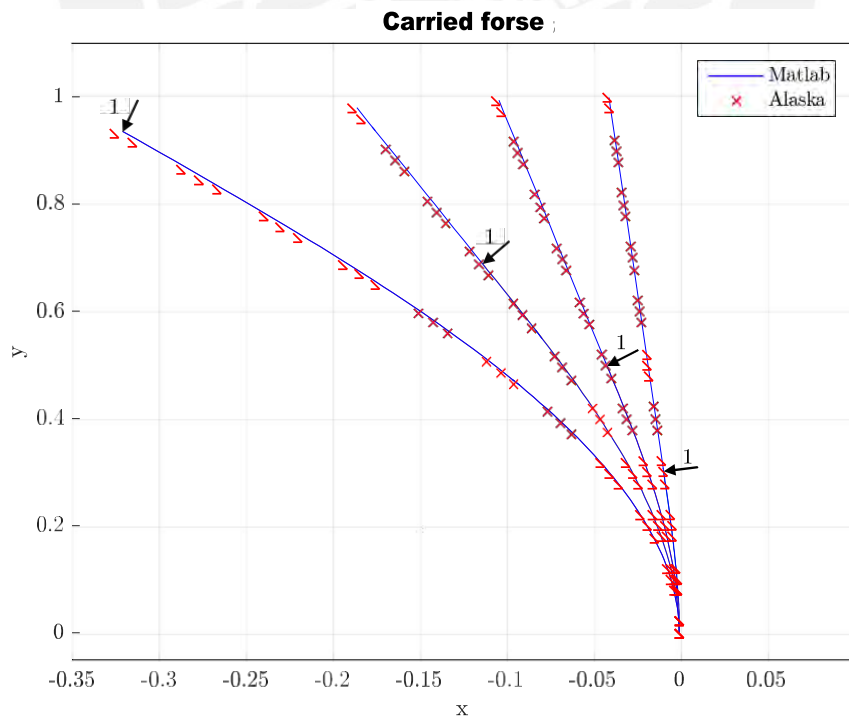


Figure 5.11: Deformation with entrained force at varied point of force application.

In fig. 5.12 and fig. 5.13 a directional force is imprinted. The force has only an x-component, so the force vector must be above the tangent of the beam.

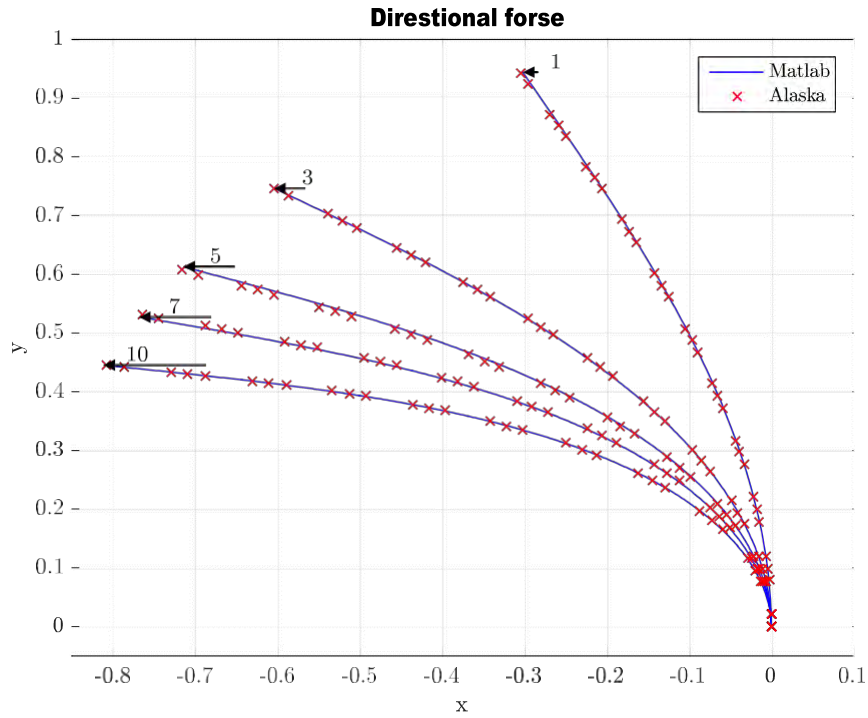


Figure 5.12: Deformation with directional force with varied amount of force.

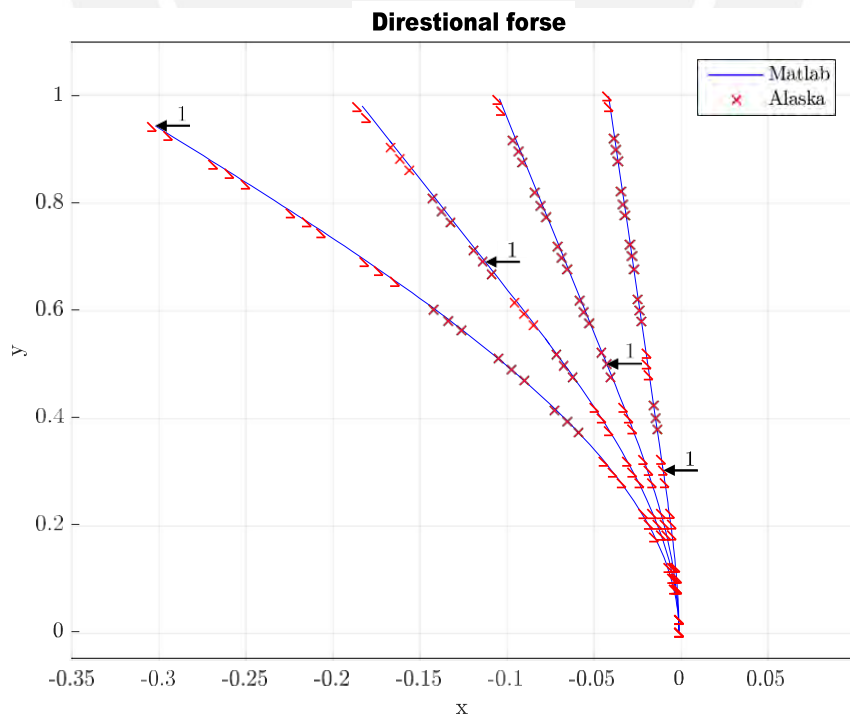


Figure 5.13: Deformation with entrained force at varied point of force application.

When comparing the results of both simulation methods, small deviations are evident. These deviations can be explained by small dynamic effects and the discretization of the Alaska model. Furthermore, a minimal length change of the beam is also simulated in *ALASKA*. The differences in the resulting support reactions between the two simulation methods are minor and can also be attributed to the effects described above. A table with the support reactions can be found in the appendix A.

Subsequently, an object with a semicircular profile contour was scanned. In *ALASKA* a very low speed of the base point with $v \approx 0.25 \text{ m s}^{-1}$ was chosen to minimize the dynamic effects, such as the impact due to the first contact. Furthermore, the friction in *ALASKA* was neglected. In fig. 5.14, it can be seen that the differences between the two simulations are very small.

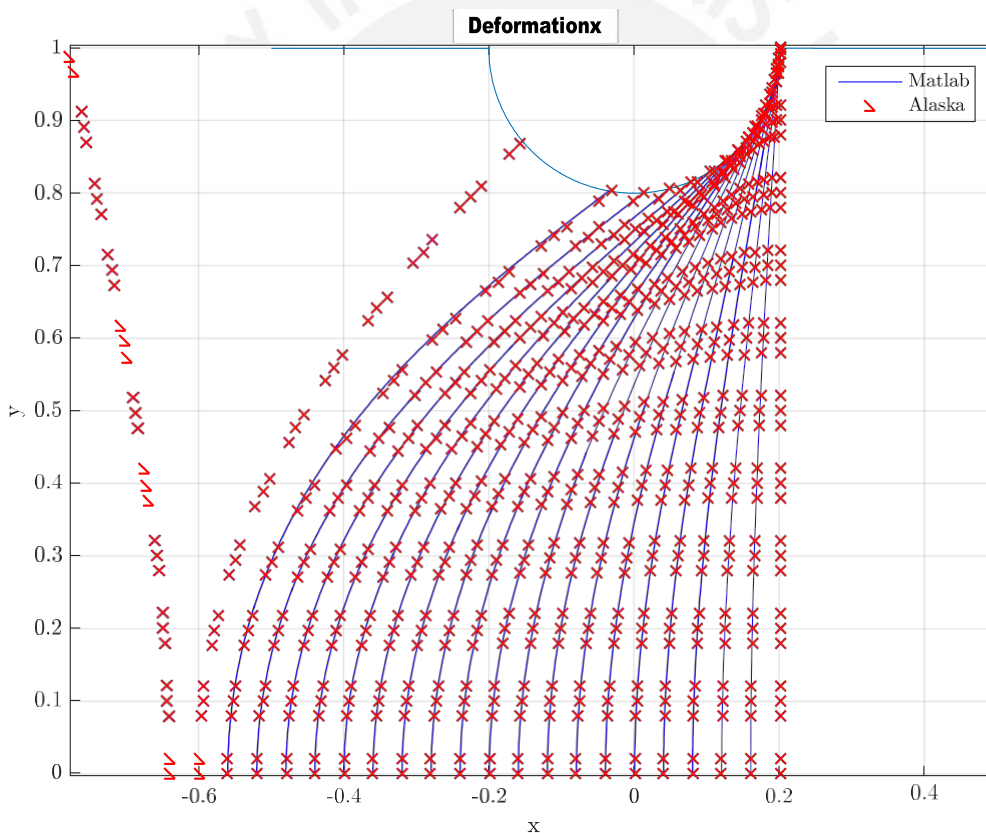


Figure 5.14: Comparison of the deformations of the vibrissae when scanning a circular contour.

The same can be seen in the results of the support reactions (see fig. 5.15). Furthermore, the dynamic separation of the vibrissa can be observed in the *ALASKA* simulation.

In the course of the support reactions it can also be seen that the simulation with *ALASKA* is in contact with the object for a longer time. This may be due to the model structure with thrust joints.

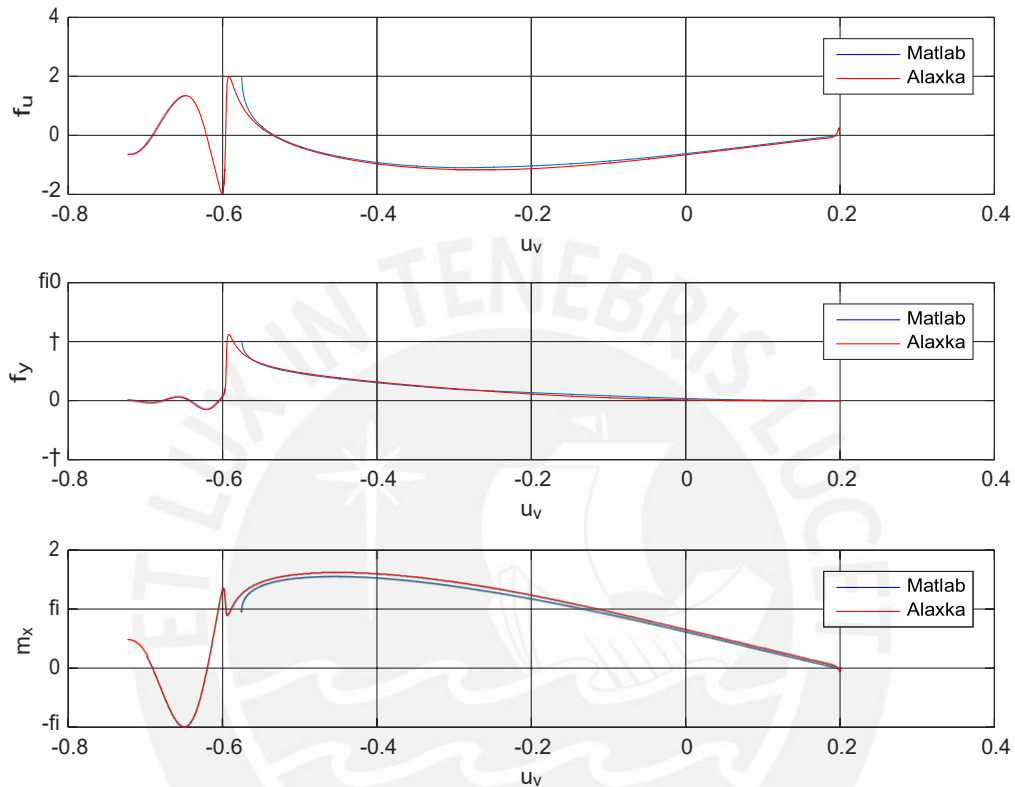


Figure 5.15: Comparison of the support reactions when scanning a circular contour.

As a final check, an object contour was scanned using a beam with an upstream spring. This corresponds to the model FB (see section 5.4.1). In *ALASKA* a „bushing element“ was used for this. This has a stiffness matrix whose entries in all spatial directions, except the x direction, are set to infinity ($\tilde{\infty}$). For the x -direction a stiffness of 70 was chosen. The corresponding support reactions are shown in figure 5.16. Again, the deviations of both simulation models are small. Furthermore, the dynamic effects when the beam is detached with the program *ALASKA* can be seen.

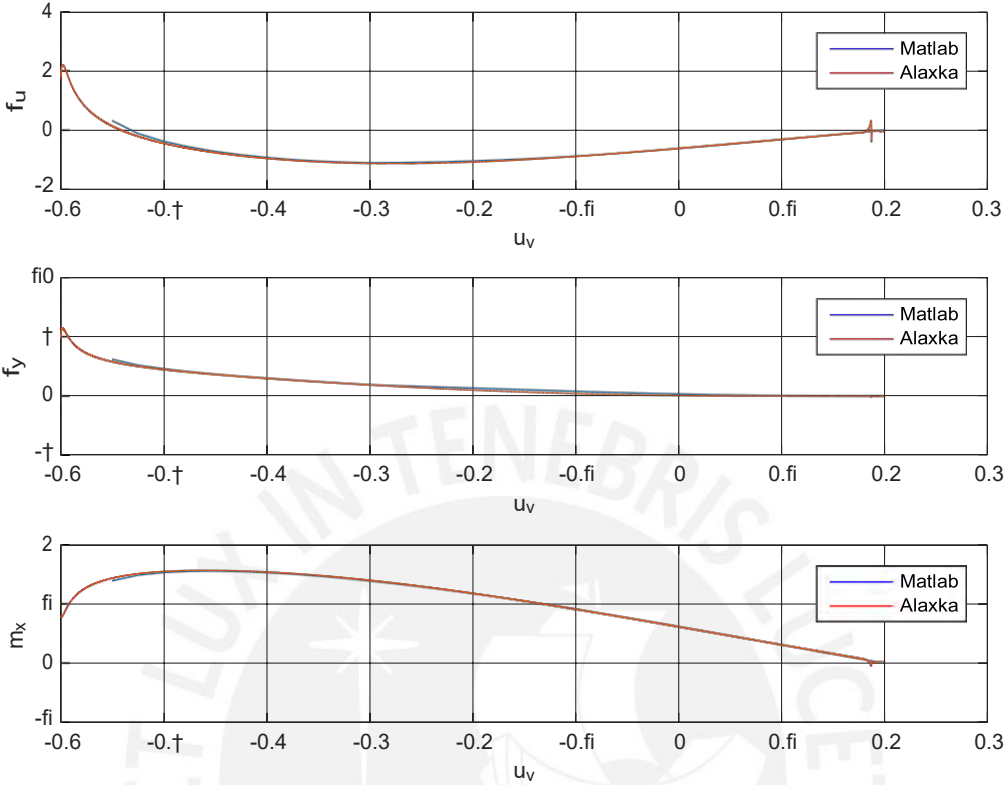


Figure 5.16: Comparison of the support reactions when scanning a circular contour with spring support.

Results

In the context of this chapter, the results of the simulation will be evaluated and subsequently discussed. In order to clarify the influences of the different parameters (spring stiffness c_i , relaxed length of the spring/vibrissae distance λ_0 and object distance q) on the support reactions, parameter studies are carried out. For the evaluation, the support reactions and the changes of the spring length Δs as a function of the manipulated variable x_v are displayed. For all simulations a step size $\Delta x_v = 0.001$ is selected. Theoretically, this value can be reduced as required, however, this leads to an increase of the simulation time. For a better visualization, the support reactions of beam 1 and beam 2 are shown side by side. The same colors in the diagrams belong to one simulation each.

In the chapter on modelling (see chapter 5), the equations required for the general case of different spring stiffnesses and spring lengths were set up. The following assumptions are made for all subsequent simulations:

- All springs have the same relaxed length ($\lambda_i = \lambda_0$).
- All springs have the same stiffness ($c_i = c_x$).

A parabolic object contour $x \in \mathbb{R} \rightarrow g(x) = ax^2 + bx + q$ with the parameters $a = 1$, $b = 0$ and $q = 0.2$ was chosen as an example for the investigations. The parameter q describes the object distance and is therefore one of the parameters to be examined.

6.1 Results for model FB

In this section, parameter studies on object scanning using the model FB (see chapter 5.3.1) are performed.

6.1.1 Variation of the spring stiffness

The stiffness of the upstream spring is subsequently varied (object distance q and relaxed length of the spring λ_0 are constant). Figure 6.1 shows four selected deformation states of the beam during the scan. The base of the beam is marked by a blue cross and the manipulated variable x_p by a black cross.

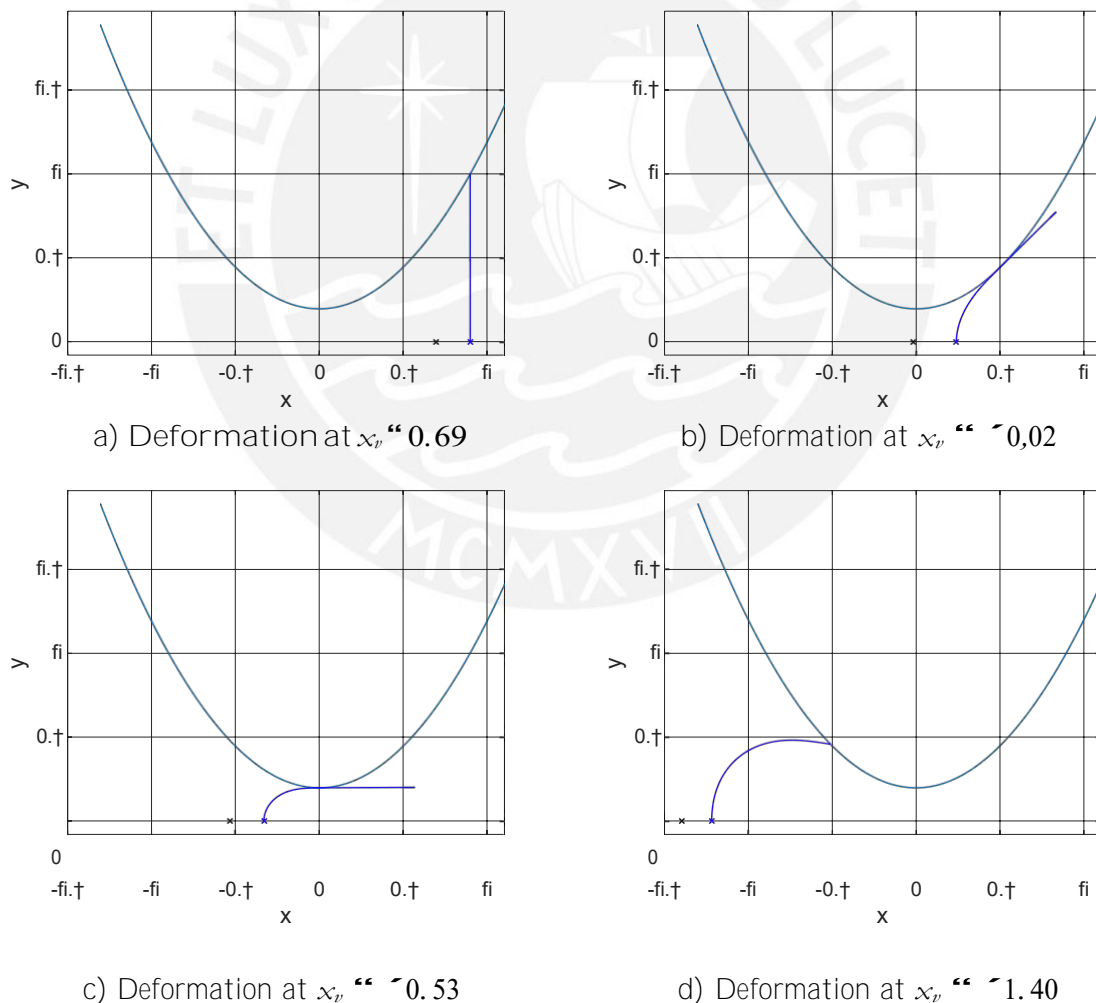


Figure 6.1: Deformation states when scanning an object with model FB:

- First contact between object and beam (peak contact);
- Tangential contact;
- Tangential contact at the vertex of the object (object slope and x component of the force f is zero);
- Tip contact immediately before detachment.

The support reactions in the clamping during object scanning are dependent on the spring stiffness c_x in Fig. 6.2 over x_v . For comparison, the support reactions are shown for a spring stiffness $c_x = \infty$. It is noticeable that the maximum values of the support reactions remain unchanged when the stiffness changes. Therefore, the maximum values cannot be influenced by a spring arrangement in x direction. Instead, a displacement of the maxima in negative x_v direction can be seen. This is caused by the length change Δs of the upstream spring during scanning. This effect occurs increasingly with decreasing stiffness. As the spring stiffness decreases, the curve is compressed, which is particularly noticeable in the support reactions f_y and m_x at a spring stiffness $c_x = 30$. With decreasing spring stiffness, the spring must be increasingly preloaded to pull the beam under the object vertex. If the spring is stiffer, the signals show a steeper increase.

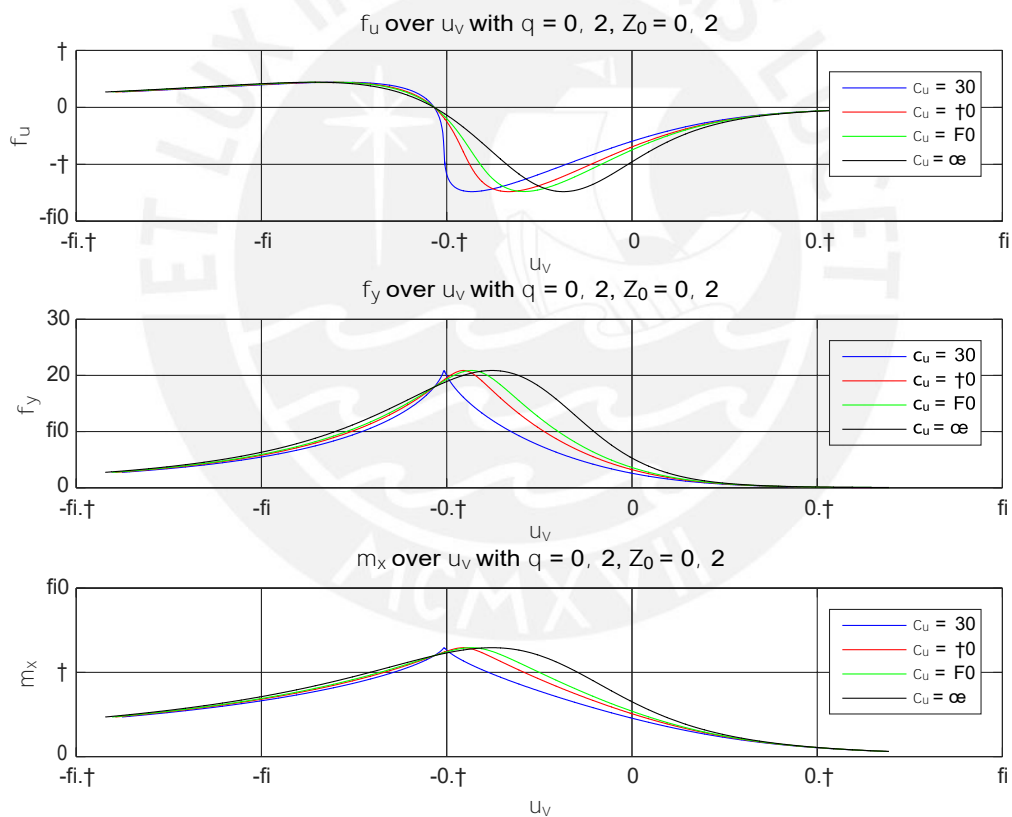


Figure 6.2: support reactions over x_v for model FB with varied spring stiffness c_x .

Furthermore, the influence of the spring stiffness can also be seen in the change in length Δs of the spring (see fig. 6.3). If the spring is softer, the change in length Δs during the scanning process is also greater. Thus, if the spring stiffness $c_x = \infty$ is infinite, the spring

length during the entire scanning process corresponds to the relaxed length of the spring ($\lambda = \lambda_0$).

In figure 6.1 b) the contact point is located at the vertex of the object. In this state, the increase in the object contour and thus the x component of the contact force f is zero. In this case there is no change in length Δs of the spring, independent of the spring stiffness c_x – thus $\lambda = \lambda_0$. This results in a common vertex of all curves in fig. 6.3 at $x_v \approx 0.53$. This can also be seen in the position reactions (see fig. 6.2) in the form of an intersection. As can be expected, the amount of this intersection is zero for the force in x direction.

While the spring is stretched on the right side of the point of intersection, it is compressed on the left side of the point of intersection.

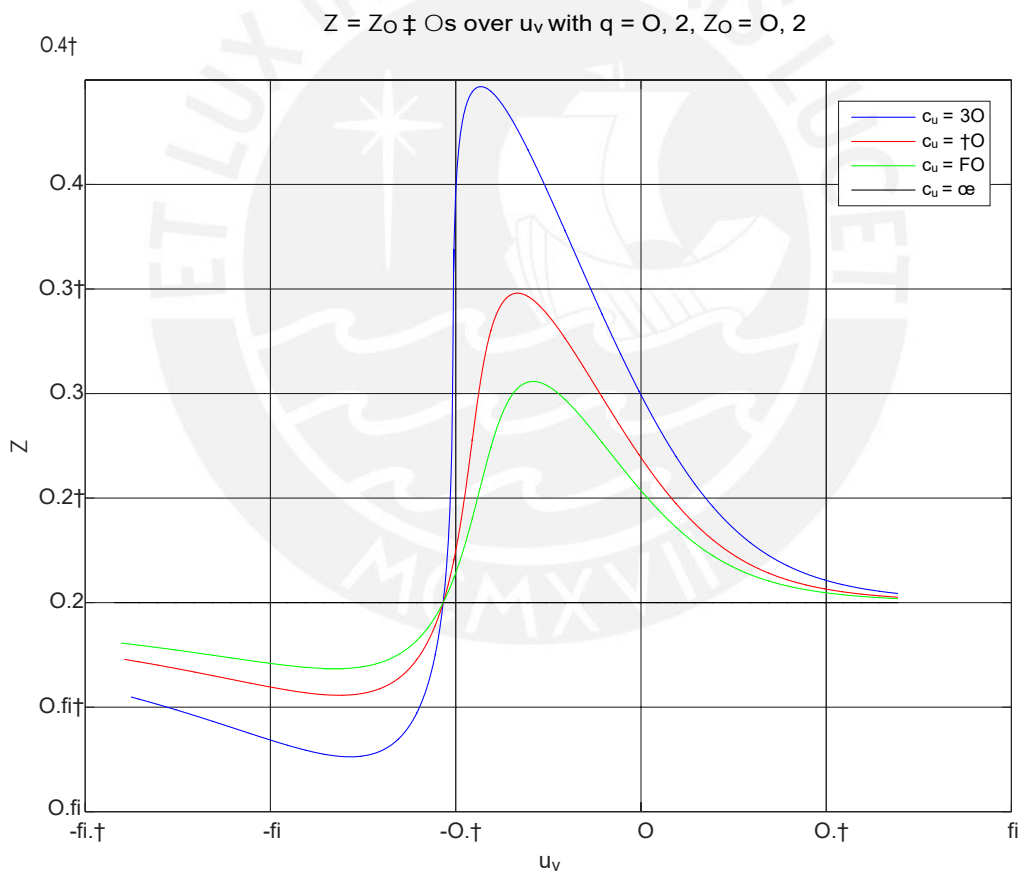


Figure 6.3: Spring length λ over x_v for model FB, with varied spring stiffness c_x .

6.1.2 Variation of the object distance

In the following, the object distance q is varied with constant spring stiffness c_x and relaxed length of the spring $\lambda_0 = 0.2$. Since the case $c_x = 8$ corresponds to a rigid bearing and this has already been extensively investigated in the context of object scanning [MBSZ19], the stiffness $c_x = 70$ is used here as an example.

In contrast to fig. 6.2, the variation of the object distance influences the maximum values of the support reactions (see fig. 6.4). The qualitative progression, however, remains largely unchanged. These findings correspond with simulation results existing in the literature [MBSZ19]. In addition, a slight trend can be seen with regard to the shifting of the maxima. As the distance to the object decreases, the maxima of the support reactions shift to the right. Furthermore, the beam jumps off the object earlier as the distance to the object increases. In contrast to the results from section 6.1.1, there is no common intersection point when varying the object distance q .

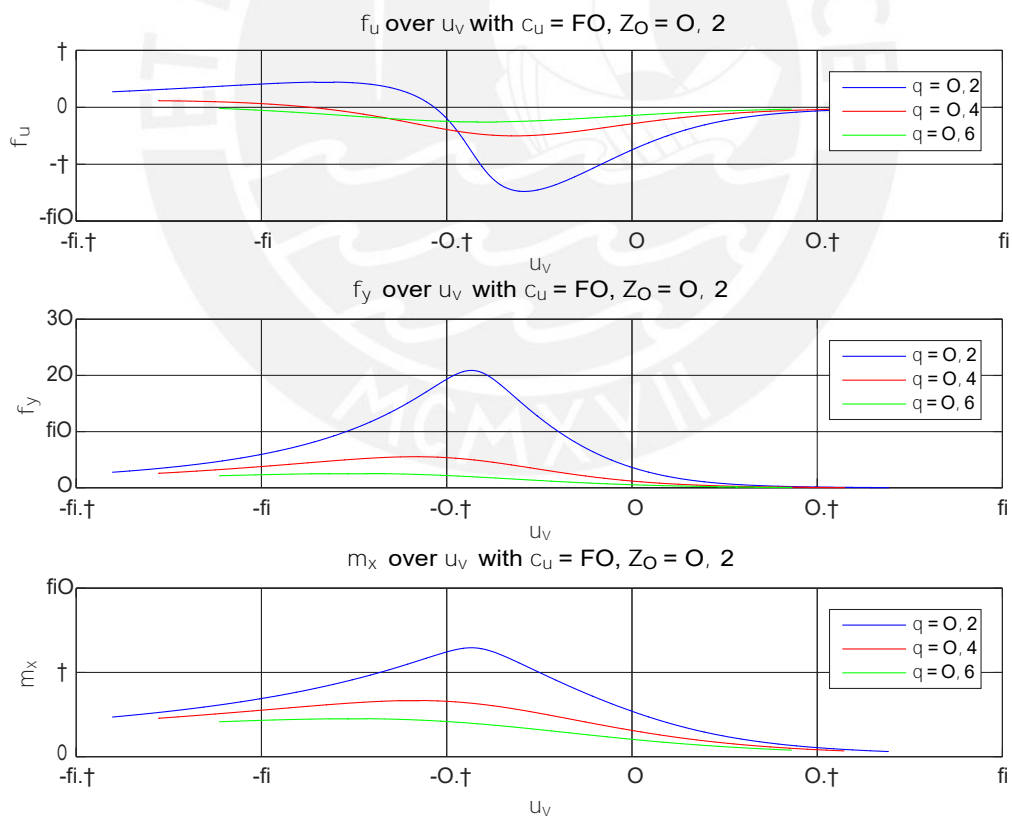


Figure 6.4: support reactions over u_v for model FB, with varied object distance q .

The same applies to changing the spring length Δs . The change in the maximum values is due to the decrease in the amount of force f when the distance q increases.

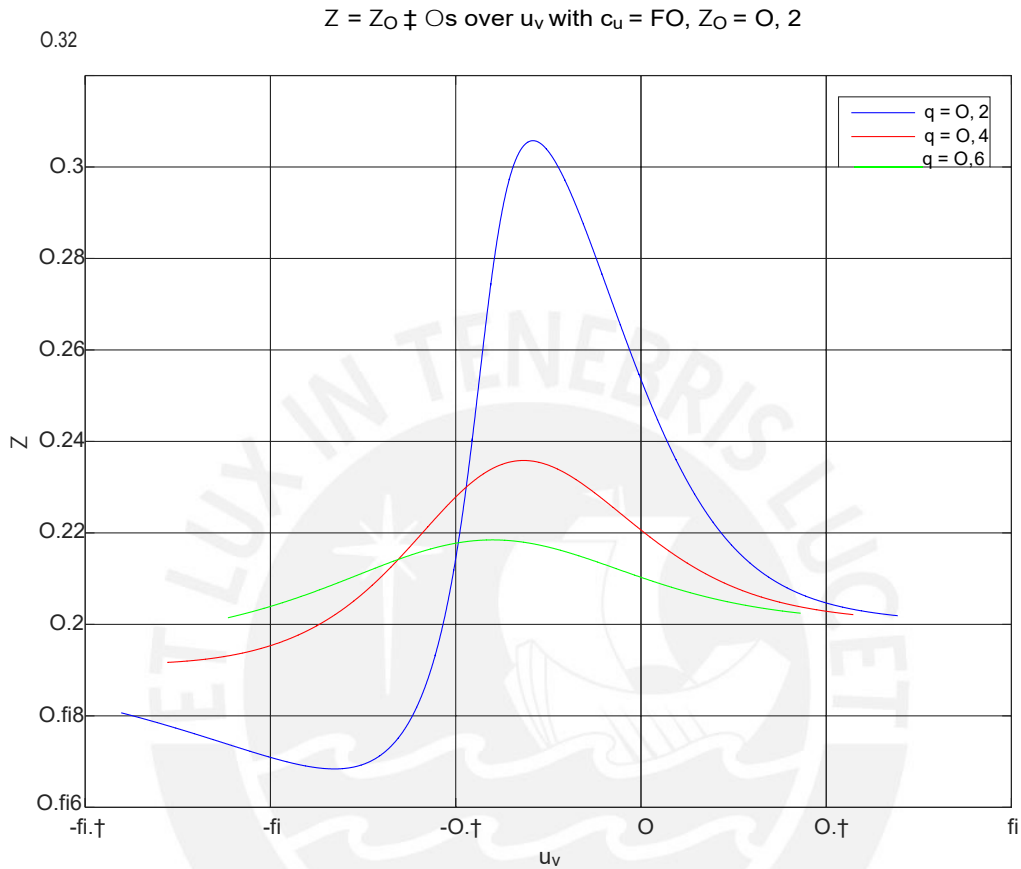


Figure 6.5: Spring length λ over x_r for model FB, with varied object distance q .

6.1.3 Variation of the relaxed length of the spring (beam distance)

Biologically, mystacial vibrissae are arranged in fields (see chapter 2). Since animals differ both among themselves and with respect to other species, the distance between adjacent vibrissae is different. For this reason a variation of the relaxed length of the spring/beam distance λ_0 is performed in the following.

A variation of the relaxed length of the spring λ_0 only leads to a shift of the signals (offset in x_r direction) in the bearing reaction, which is caused by the delayed contact between beam and object. The course and maximum values remain unchanged (see fig. 6.6).

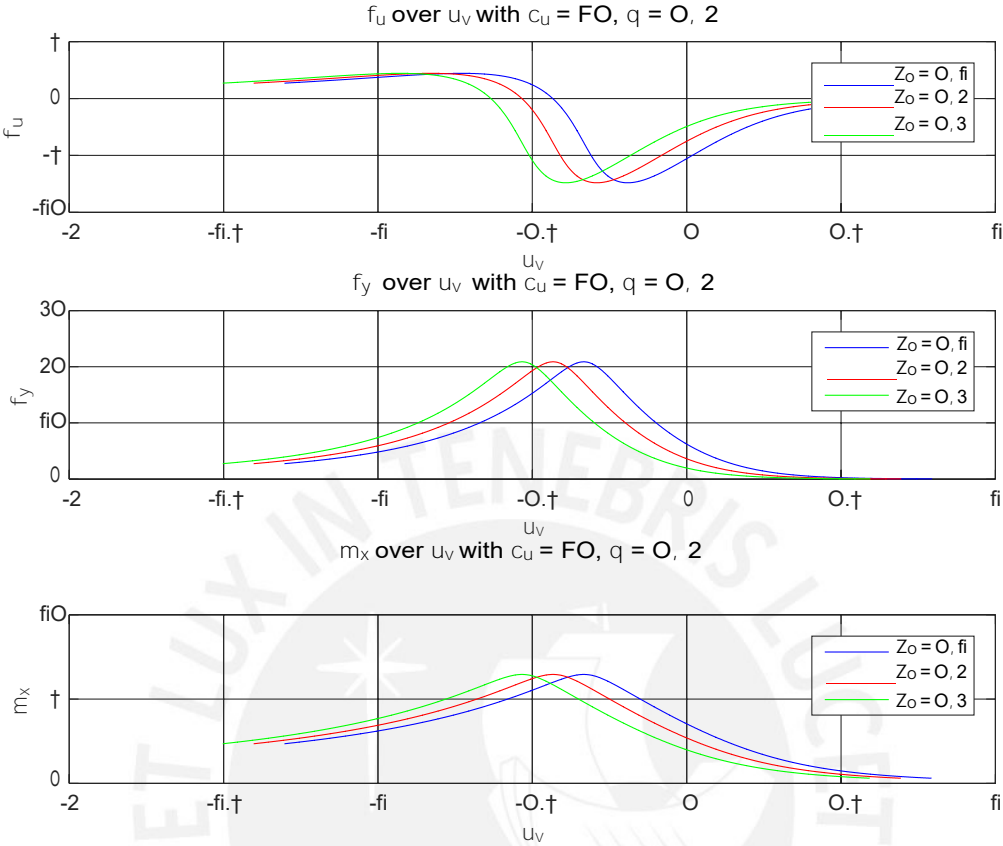


Figure 6.6: support reactions over x_v for model FB, with varied relaxed length of the spring λ_0 .

In the diagram of spring lengths (see fig. 6.7), two effects can be noted. Firstly, there is an offset of the maximum values which can be directly assigned to the relaxed length of the spring. On the other hand, a displacement in x direction can be seen. This effect shows, as already in the support reactions (see fig. 6.6), the delayed contact between beam and object.

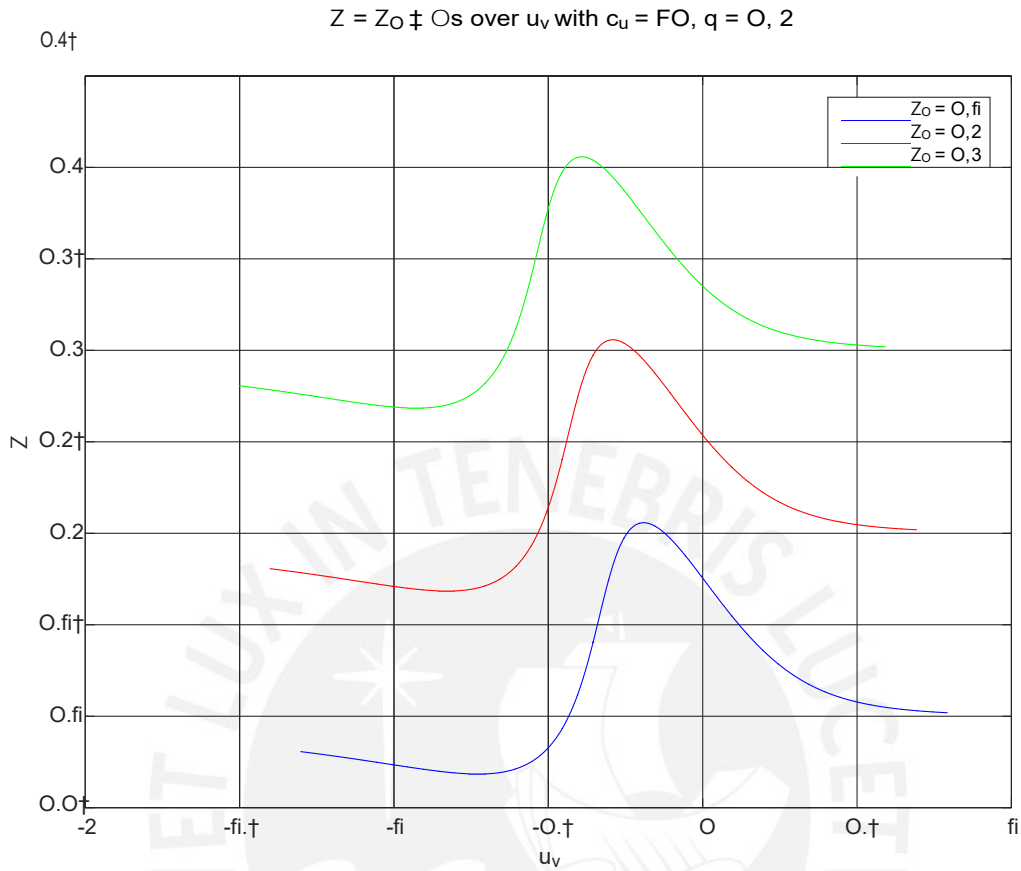


Figure 6.7: Spring length λ over x_v for model FB, with varied relaxed spring length λ_0 .

6.2 Results for model FBFB

In the following the results of the simulation of two coupled beams with an upstream spring will be examined.

Figure 6.8 shows a selection of deformation states during the scanning process. The base points (x_{01} , x_{02}) and the manipulated variable x_v are shown as crosses. The manipulated variable x_v is black, beam 1 with the corresponding base is blue and beam 2 with the base is red. In addition to the deformations, the change in the distances between the individual base points can also be seen in this display.

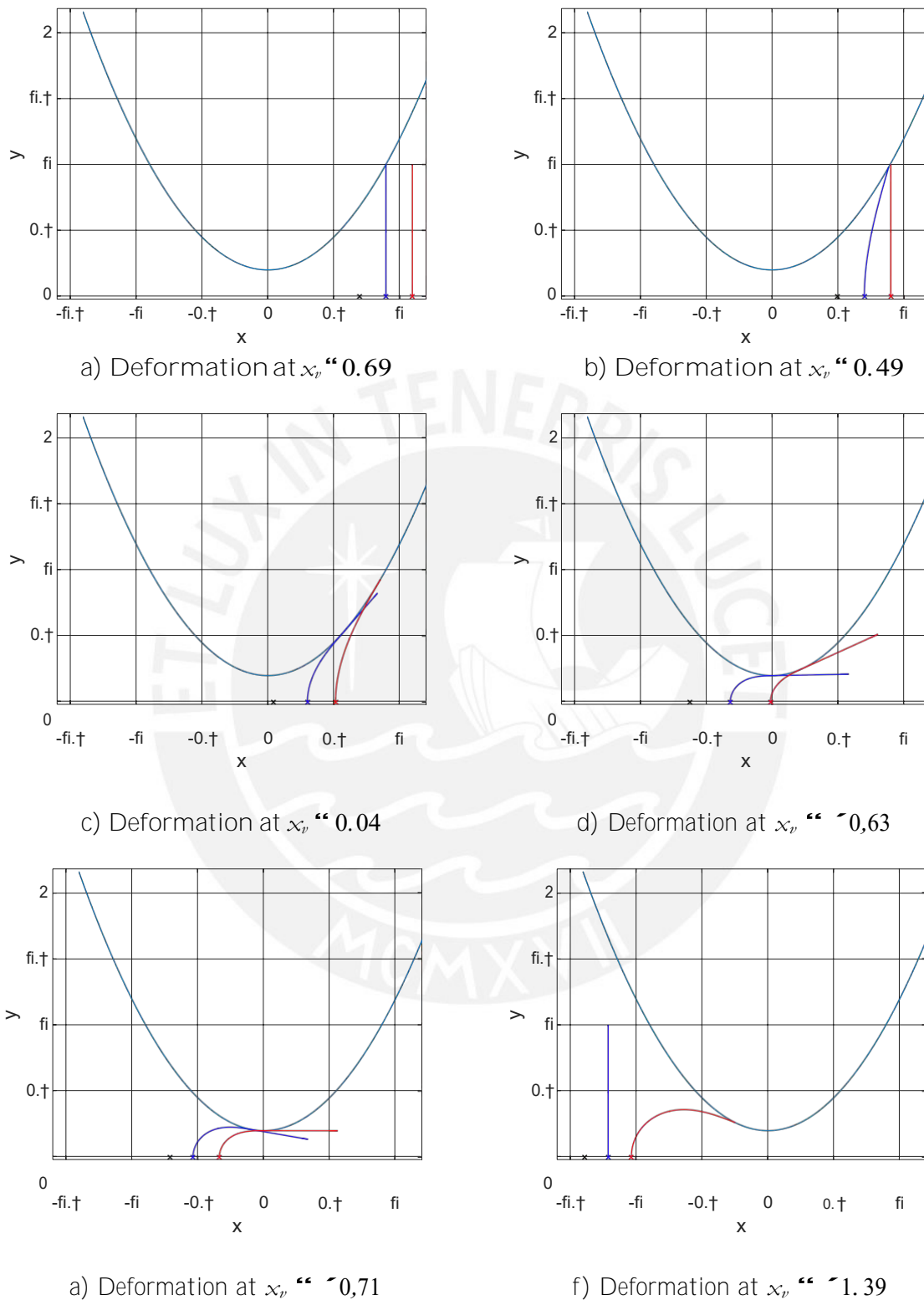


Figure 6.8: Deformation states when scanning an object with model FB: a) First contact between object and beam 1; b) First contact between object and beam 2; c) Both beam are in contact with the object; d) Tangential contact of beam 1 at the vertex of the object (object rise and x components of force \mathcal{F}_1 is zero); e) Tangential contact of beam 1 at the vertex of the object (object slope and x -component of force \mathcal{F}_2 is zero); f) beam 1 jumped off, beam 2 is in contact with the object.

Figure 6.9 shows the course of the support reactions of both beams via the manipulated variable x_r . The components of the support reactions for both beams have the same maximum values. Due to the distance between the two beams, they occur one after the other, first for beam 1 and then for beam 2. Furthermore, the signal of beam 2 is compressed in the direction of x_r compared to that of beam 1. As soon as the contact point of beam 1 has reached the apex of the object, the direction of loading of spring 1 changes from tension to compression. Due to the coupling of the beams, this not only affects the base point position of beam 1, but also that of beam 2. The compression of the signals caused by this can be seen especially in the support reactions f_y and m_z , whose maxima are not distinguishable. Furthermore, compared to beam 1 for beam 2, the increase of all support reactions is smaller at the beginning of the sampling. This also results from the influence of the force f_1 on the base position of beam 2 x_{02} (see section 5.4.2). It is also possible to detect the detachment of beam 1 (see fig. 6.8 f) in the support reactions. The support reactions of beam 1 fall to zero (see fig. 6.9). This is based on the quasi-static simulation method. In dynamic simulations, when the beam is detached from the object, a free oscillation of the beam occurs, which influences the support reactions (see fig. 5.14). Furthermore, the detachment of beam 1 can also be seen in the support reactions of beam 2. This is exemplarily shown in a detailed view of the support reaction f_y in figure 6.10. The values of the support reactions of beam 2 change slightly because the spring circuit changes due to the detachment of beam 1.

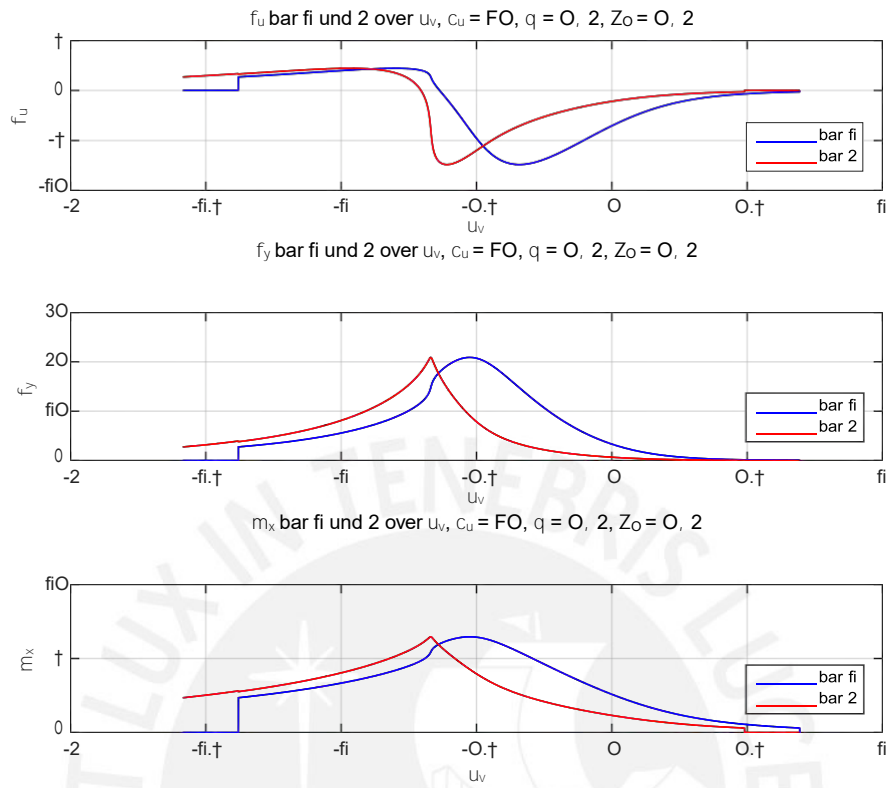


Figure 6.9: Support reactions of both beams via x_v for model FBFB.

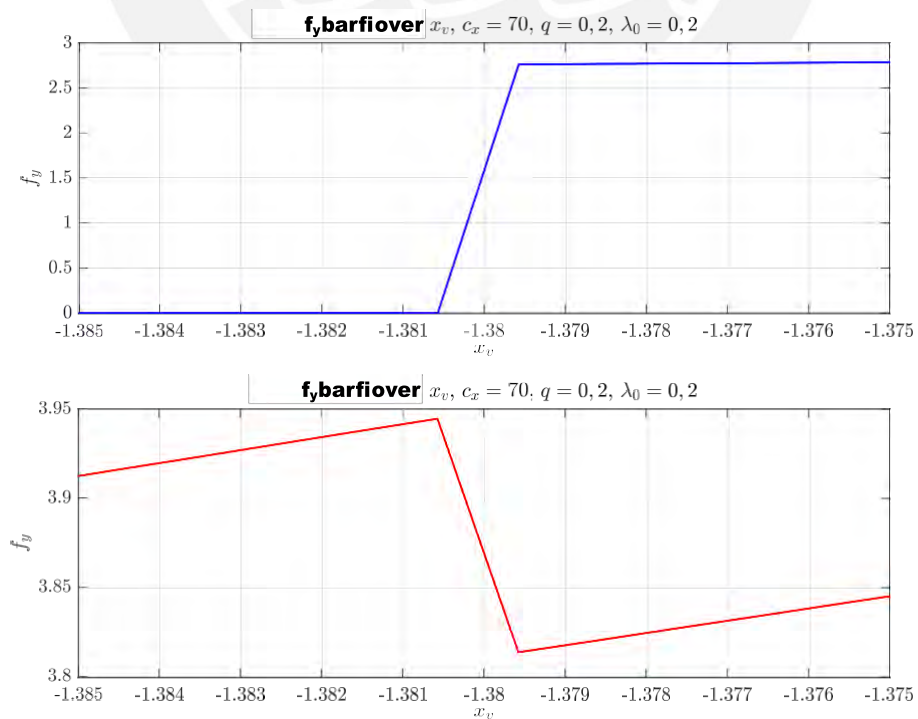


Figure 6.10: Detailed view of the force f_y of both beams when replacing beam 1 via x_v for model FBFB.

6.2.2 Variation of the spring stiffness

A variation of the spring stiffness leads in the support reactions of both beams, analogous to model FB (see section 6.1), to a displacement of the maxima in negative x_r direction. The maximum values remain unchanged.

Furthermore an earlier detachment of both beams at a spring stiffness $c_x = 50$ can be recognized.

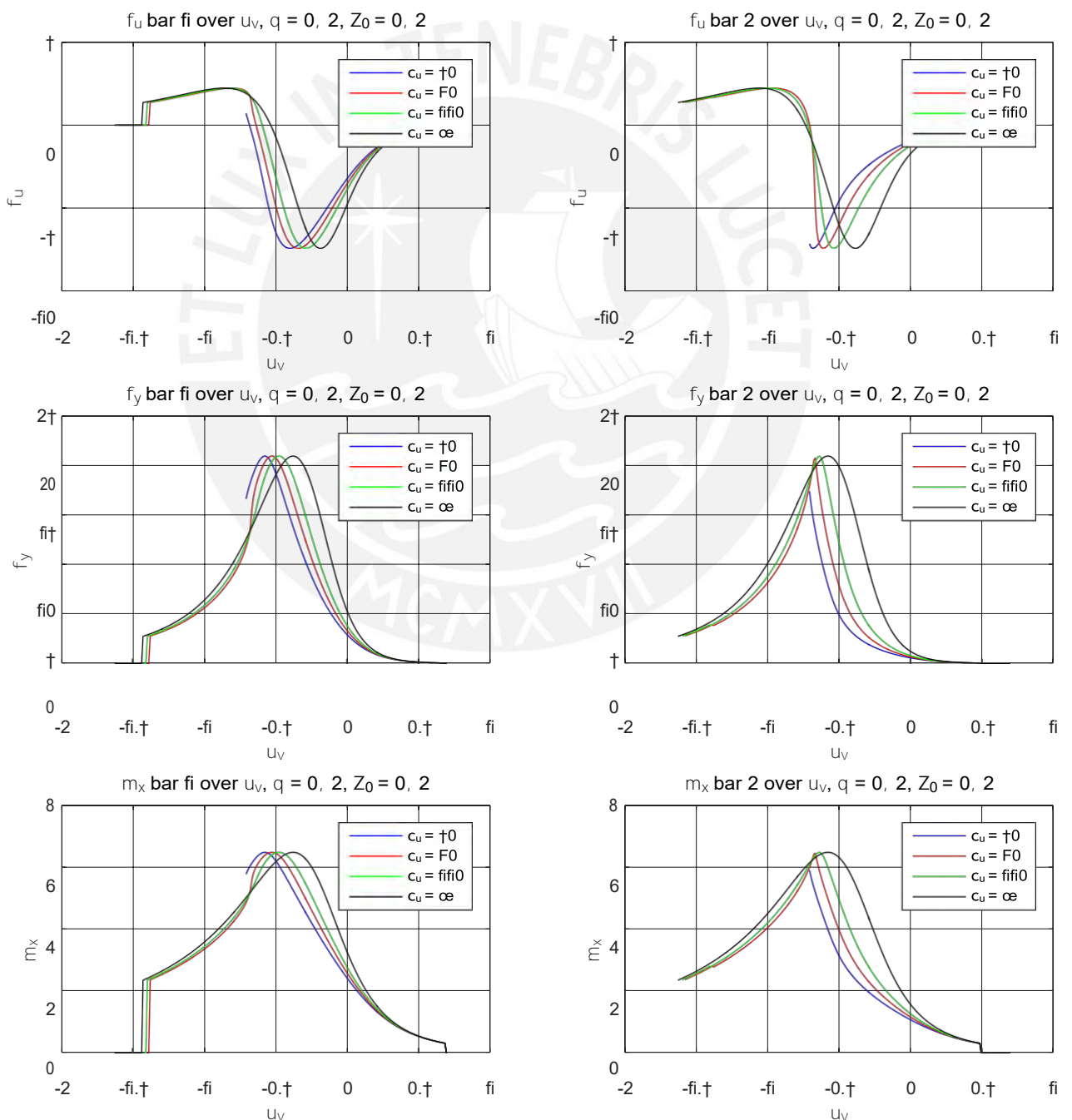


Figure 6.11: Support reactions over x_r for model FBFB, with varied spring stiffness c_x .

The change of the spring lengths Δs is also partly analogous to the model FB (see section 6.1). The changes in length Δs_i of both springs during the scanning process become larger as the spring stiffness c_x decreases.

However, there is no common point of intersection of the individual curves. This again shows the influence of the coupling to the other beam on the base point of the beam.

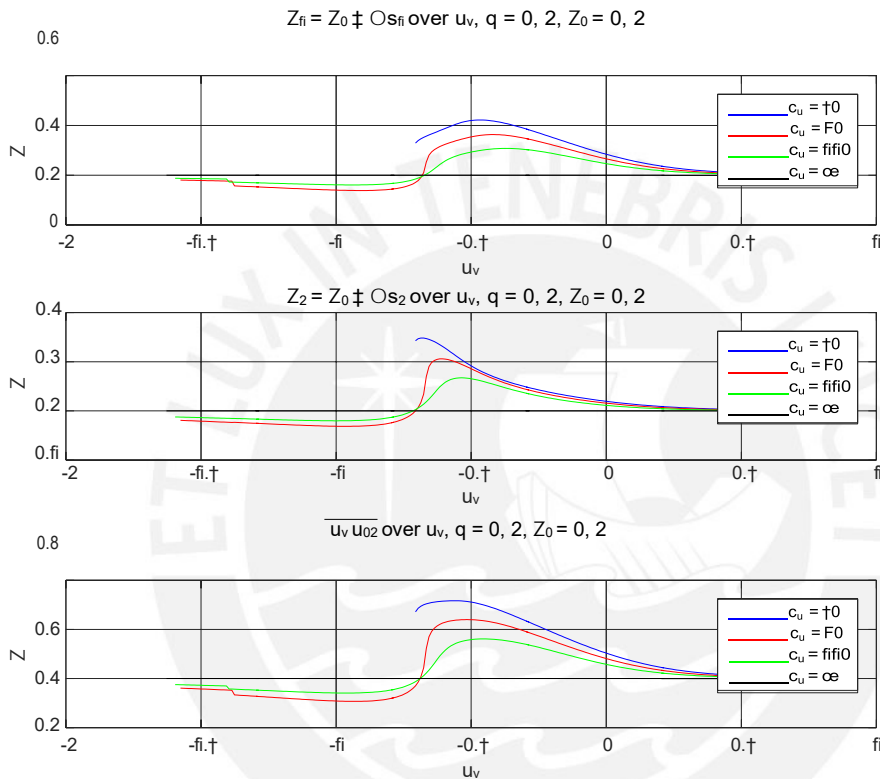


Figure 6.12: Spring lengths λ_i over x_i for model FBFB with varied spring stiffness c_x .

6.2.2 Variation of the object distance

When varying the object distance q for the model FBFB with constant spring stiffness $c_x = 70$ and relaxed length of the spring $\lambda_0 = 0.2$, a decrease in the maximum values of the support reactions must be objectified with increasing object distance q (see fig. 6.13). This finding corresponds to the results of the simulations with a beam (see section 6.1.2). Also the trend of the maximum displacement and the earlier detachment of the beams with increasing object distance q can be recognized analogously to section 6.1.

Furthermore, an increasing compression at a smaller object distance is noticeable, especially in the support reactions of the second beam. The reason for this is the higher maximum value of the force in x direction of the beam 1 f_{x1} and the corresponding coupling of the base

point of the beam 2 x_{02} . If the contact force is greater due to the smaller object distance, the base of beam 2 x_{02} slips more when passing the vertex of beam 1.

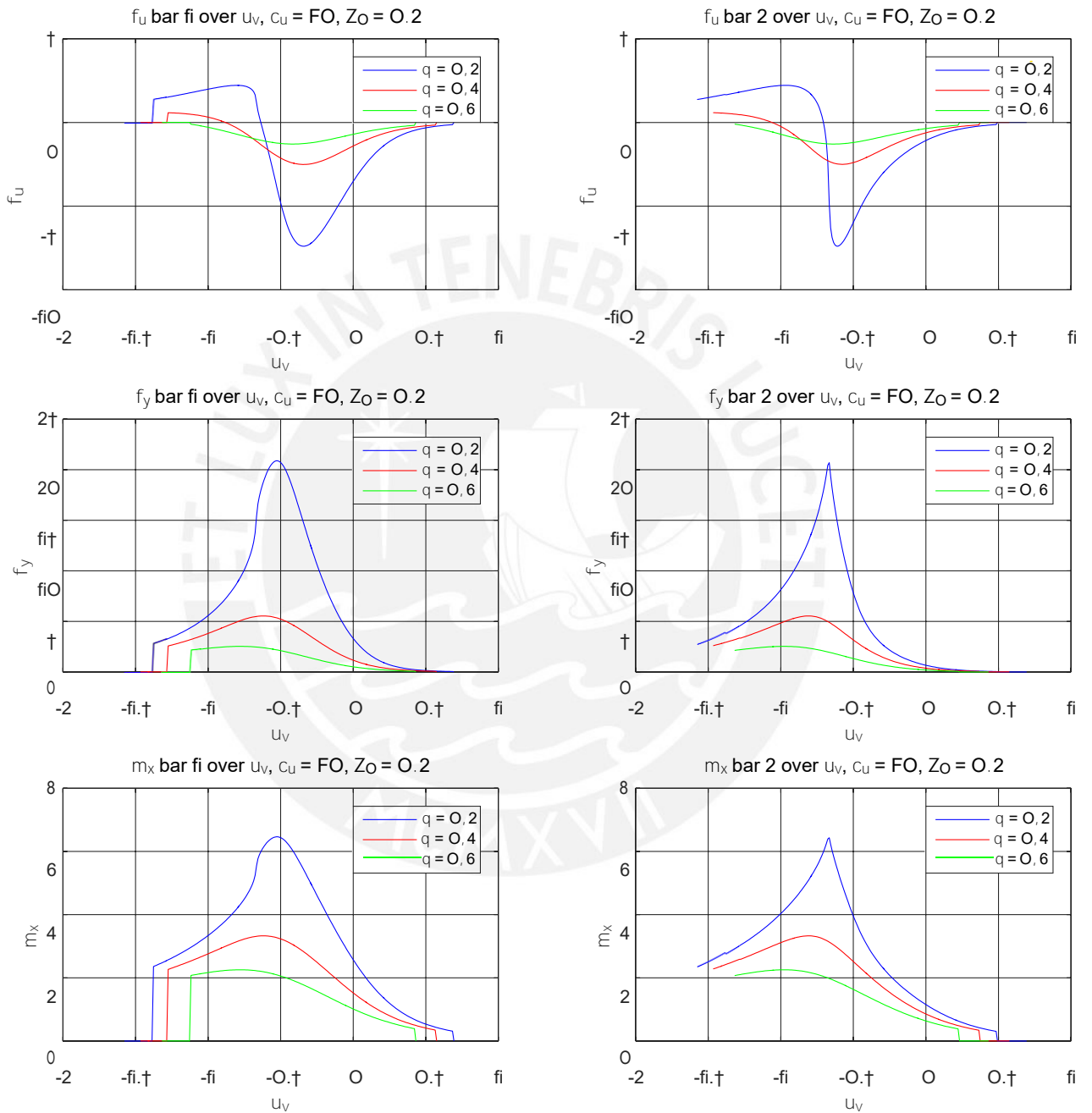


Figure 6.13: Support reactions over x_v for model FBFB with varied object distance q .

A change in the maximum values can also be seen in the length changes of the springs Δs . This is due to the decrease in contact forces f_i with increasing object distance q .

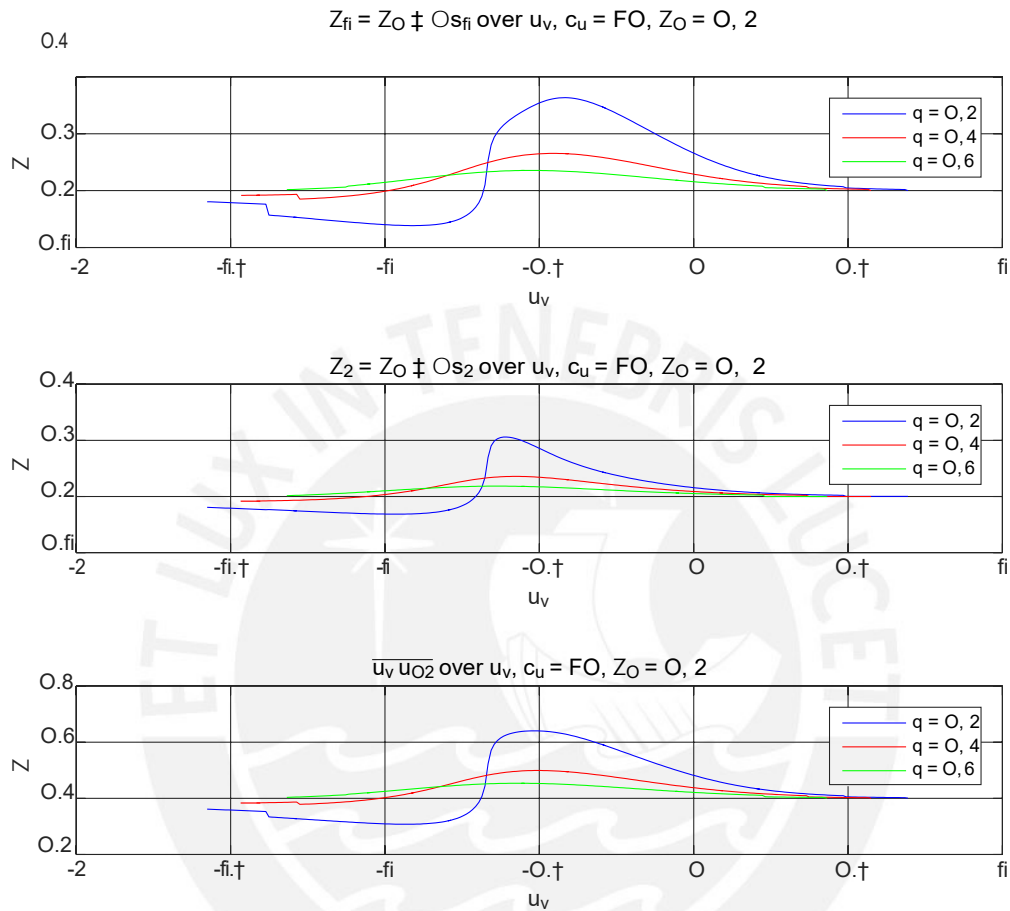


Figure 6.14: Spring lengths λ_i over x_i for model FBFB with varied object distance q .

6.2.3 Variation of the relaxed length of the spring (beam distance)

As with model FB (see section 6.1), a change of the relaxed spring length λ_0 results in a displacement of the signals (offset in x_v direction). However, the courses of the support reactions of beam 1 differ slightly. This is due to the change of the loading direction from tension to compression of spring 1 when beam 1 contacts the object's vertex.

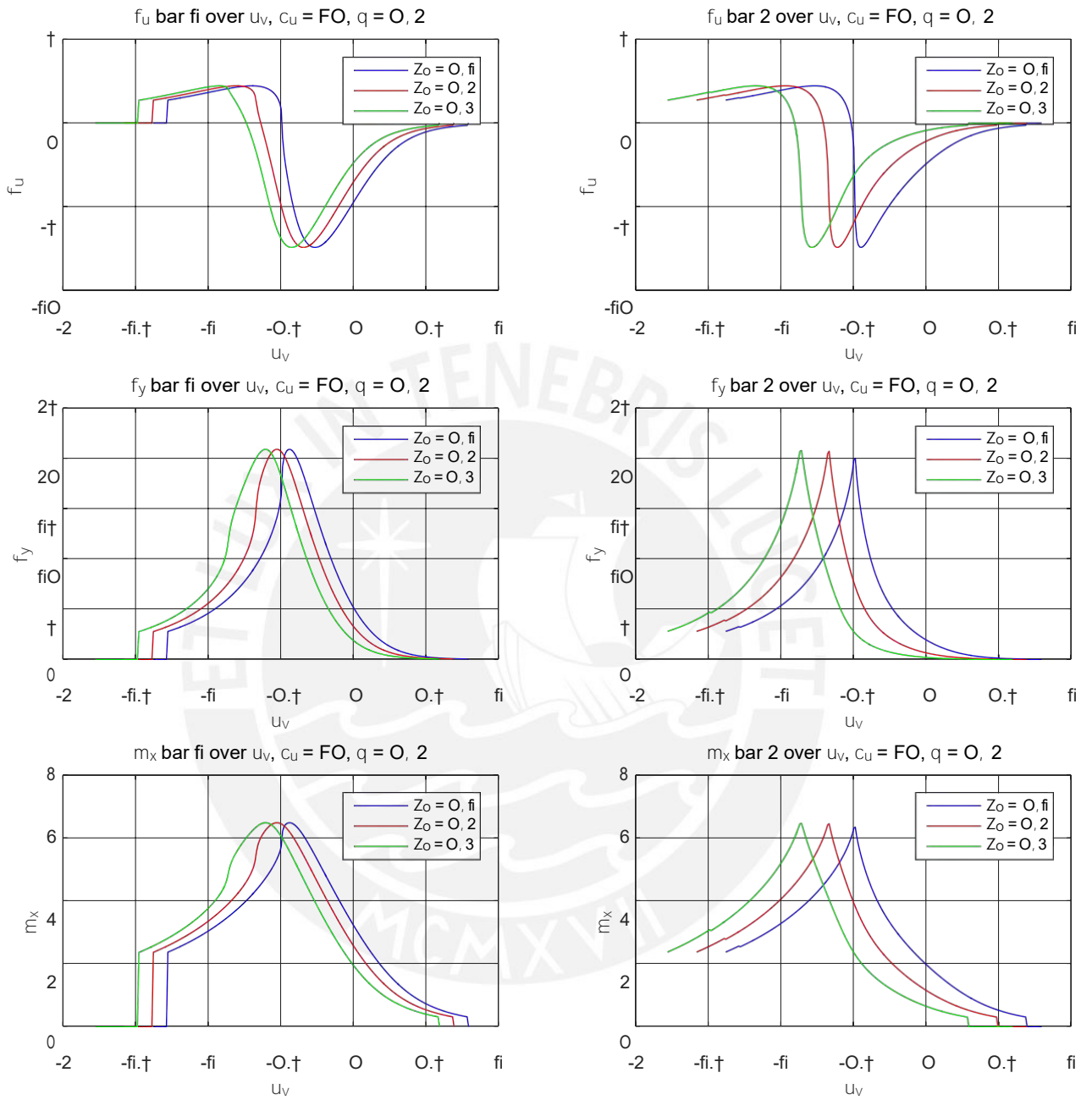


Figure 6.15: support reactions over x_v for model FBFB with varied relaxed length of the spring λ_0 .

Figure 6.24 shows the spring length when the relaxed length of the spring is varied. The changes of the maximum values and the displacement in x direction when changing the length of the spring Δs is analogous to section 6.1.3.

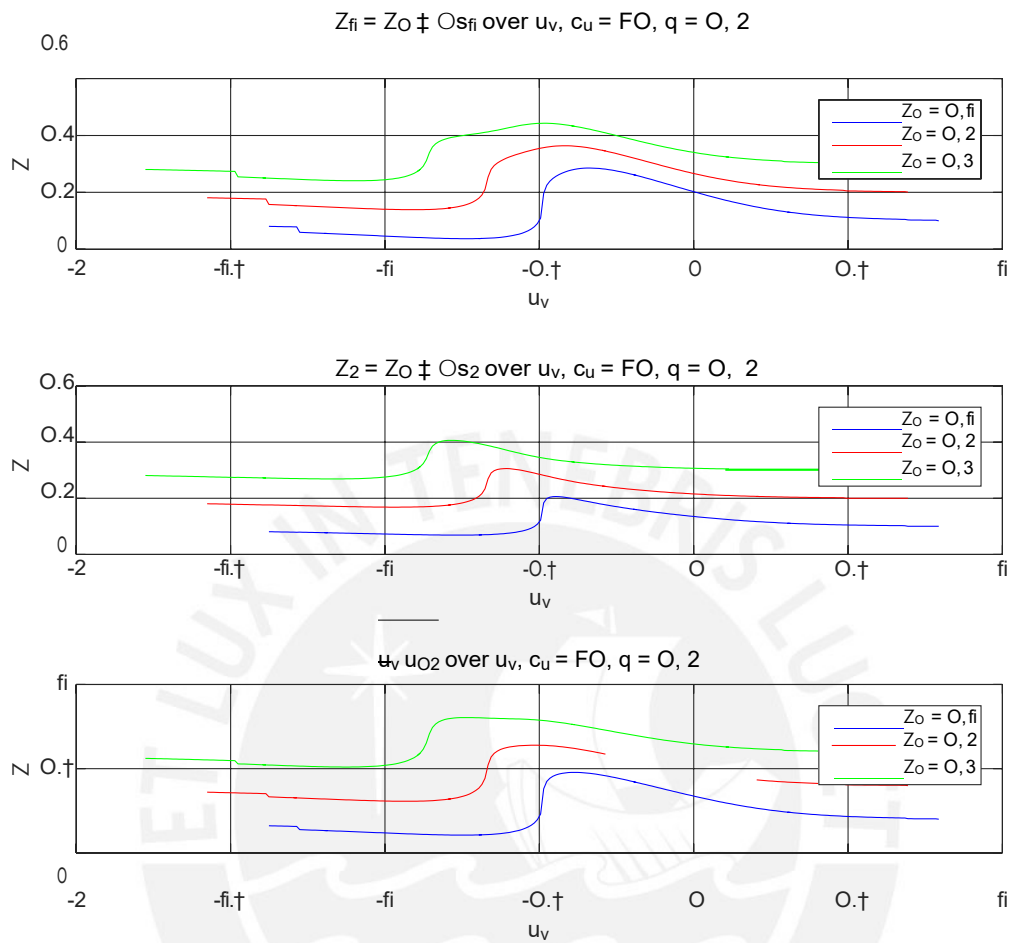


Figure 6.16: Spring lengths λ_i over x_r for model FBFB with varied relaxed spring length λ_0 .

6.3 Results for model FBFB

In the following, the results of the model of two coupled beams with upstream spring and feedback are examined (see section 5.3.3).

The figure 6.17 shows the course of the support reactions of both beams via the manipulated variable x_r for the model FBFB. Basically the effects described in section 6.2 can be recognized. However, these are less pronounced due to the counteraction of spring 3. For example, the compression of the support reactions of beam 2 is less than in model FBFB. Due to the direct coupling to the manipulated variable x_r the feedback reduces the influence of the two beams on each other. Thus the influence of the detachment of beam 1 on beam 2 is also lower (see fig. 6.18).

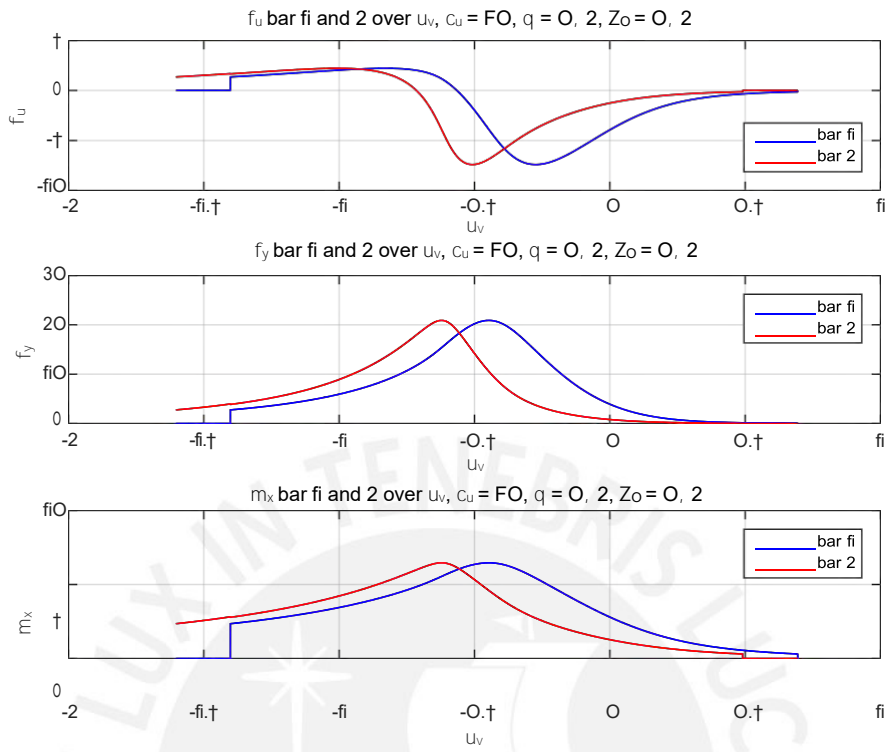


Figure 6.17: Support reactions of both beam via x_v for model FBFBR.

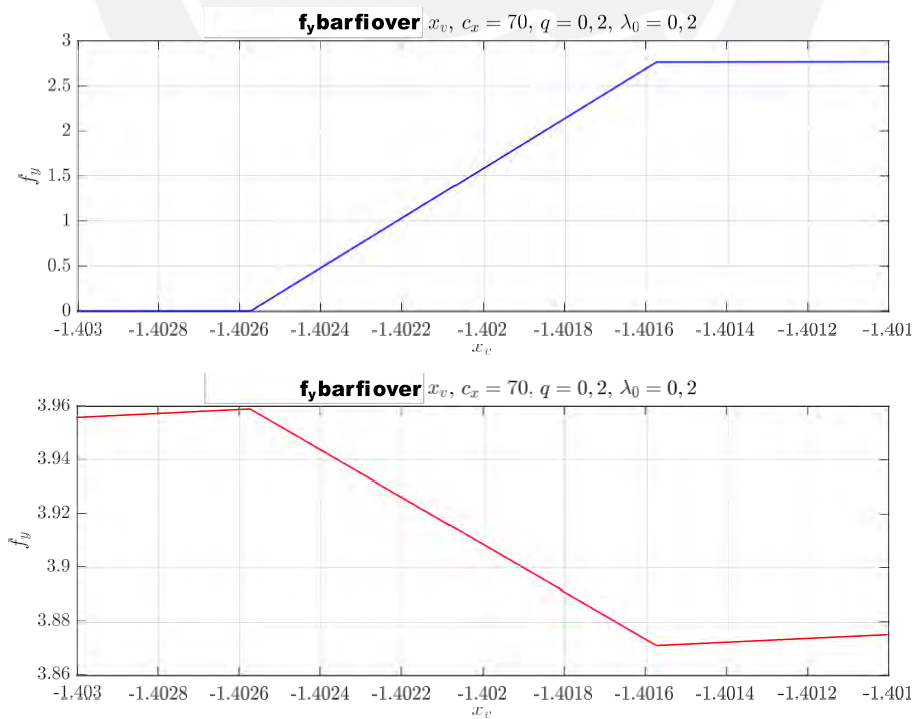


Figure 6.18: Detailed view of the force f_y of both beams when replacing beam 1 via x_v for model FBFBR.

6.3.1 Variation of the spring stiffness

Similar to the model FBFB (see section 6.2.1), changing the stiffness of the springs c_x only causes a shift in the maxima of the support reactions (see fig. 6.19). However, the displacement due to spring 3 is smaller than in the model without feedback. Also in this spring circuit, the spring stiffness does not influence the maximum values of the support reactions.

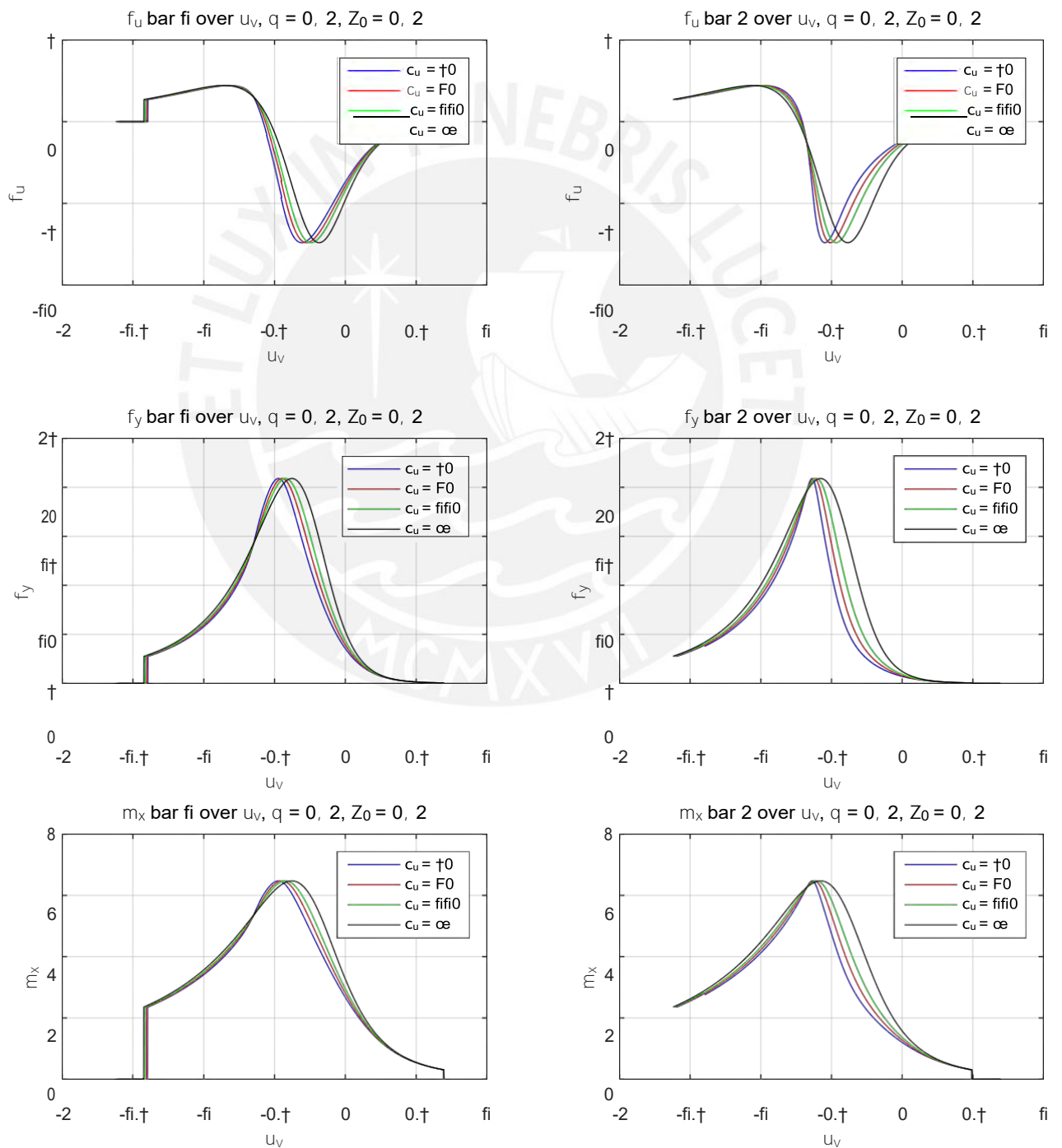


Figure 6.19: Support reactions over x_v for model FBFB at varied spring stiffness c_x .

Also when looking at the spring lengths λ_i , a lower maximum value can be seen (see fig. 6.20). Again, the effect of spring 3 is the cause.

A common intersection due to the vertex, compared to model FB (see subchapter 6.1.1), is not visible.

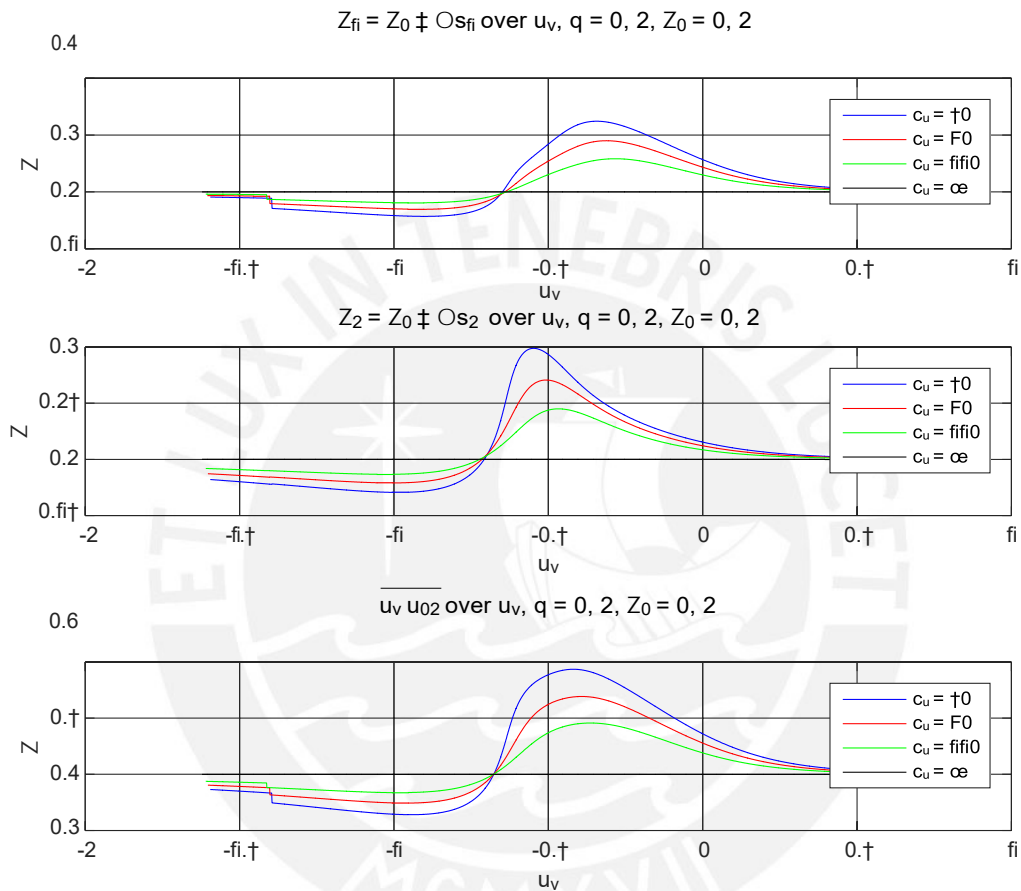


Figure 6.20: Spring lengths λ_i over x_i for model FBFBR with varied spring stiffness c_x .

6.3.2 Variation of the object distance

When varying the object distance, a smaller displacement of the signals in x direction can be seen compared to the model FBFBR (see section 6.2.2). The influence of the spring 3 reduces the base point displacement of both beams. In addition, no new effects can be seen compared to section 6.2.2.

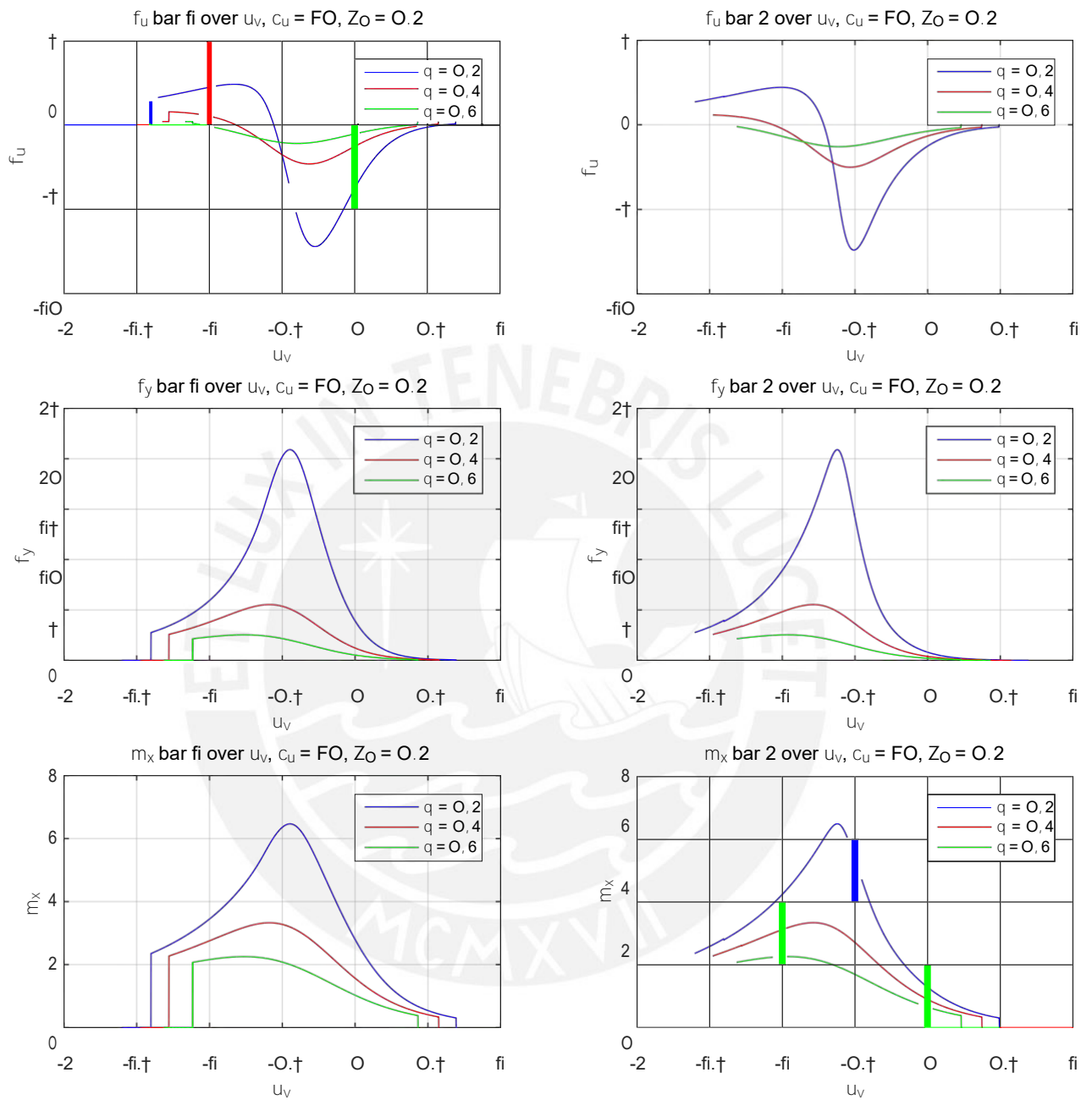


Figure 6.21: Support reactions over x_r for model FBFBR with varied object distance q .

The same analogy can also be seen in the change in length of the springs Δs (see fig. 6.22).

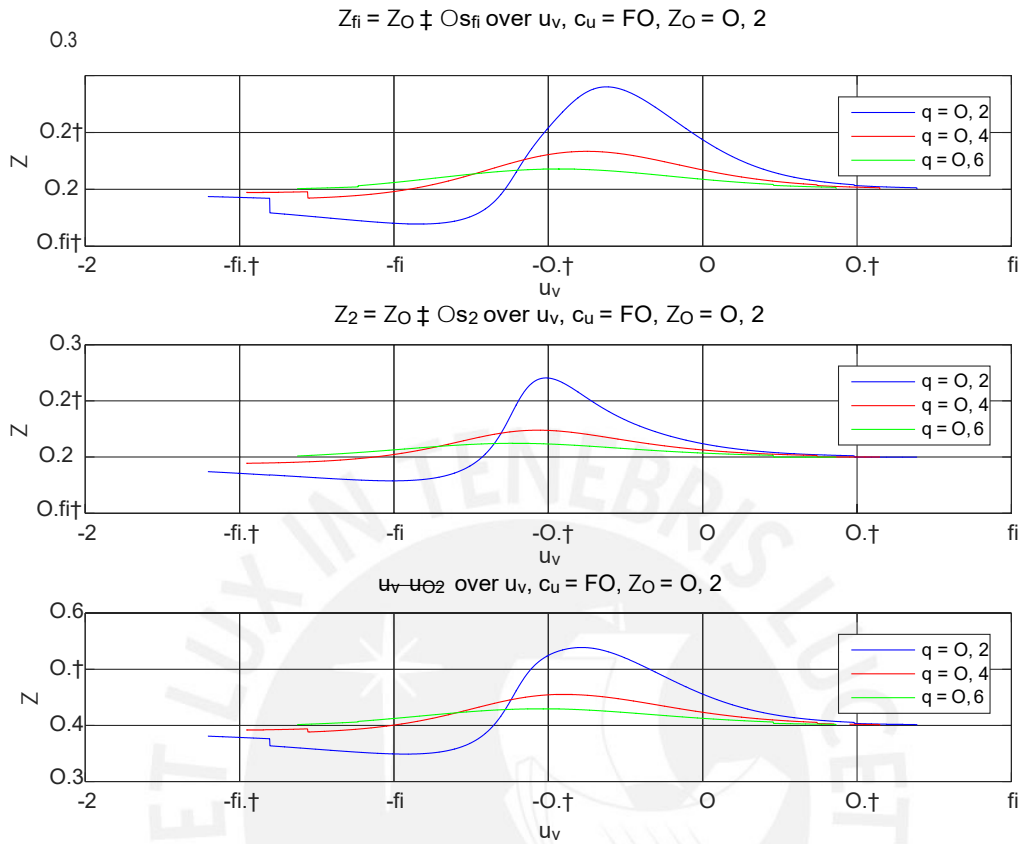


Figure 6.22: Spring lengths λ_i over x_i for model FBFBR with varied object distance q .

6.3.3 Variation of the relaxed length of the spring (beam distance)

Changing the relaxed length of the spring λ_0 only leads to a shift of the support reactions on the x axis (see fig. 6.23).

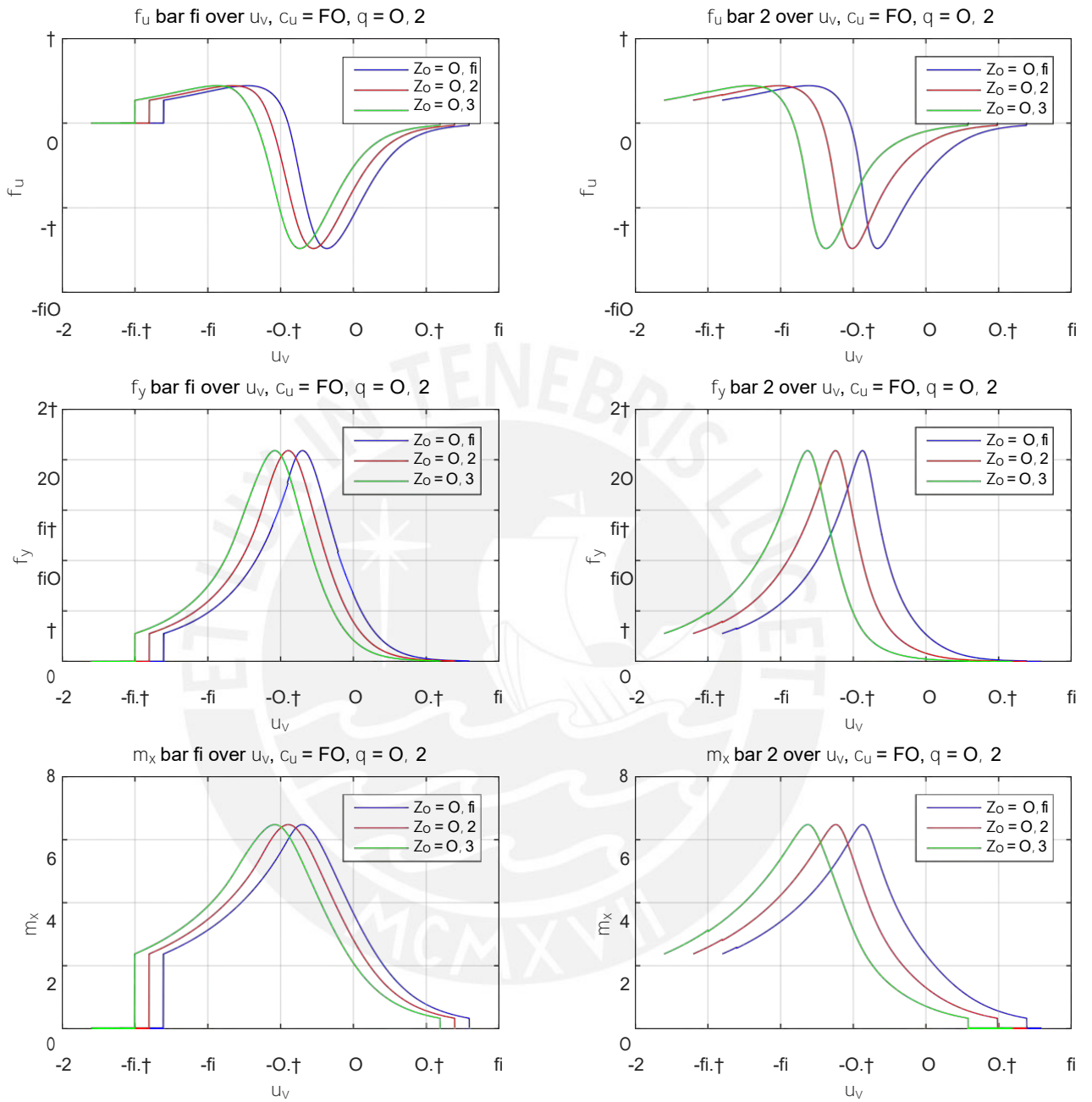


Figure 6.23: Support reactions over x_r for model FBFBR with varied basic spring length λ_0 .

This shift in x_r direction can also be seen in the length changes Δs (see fig. 6.24).

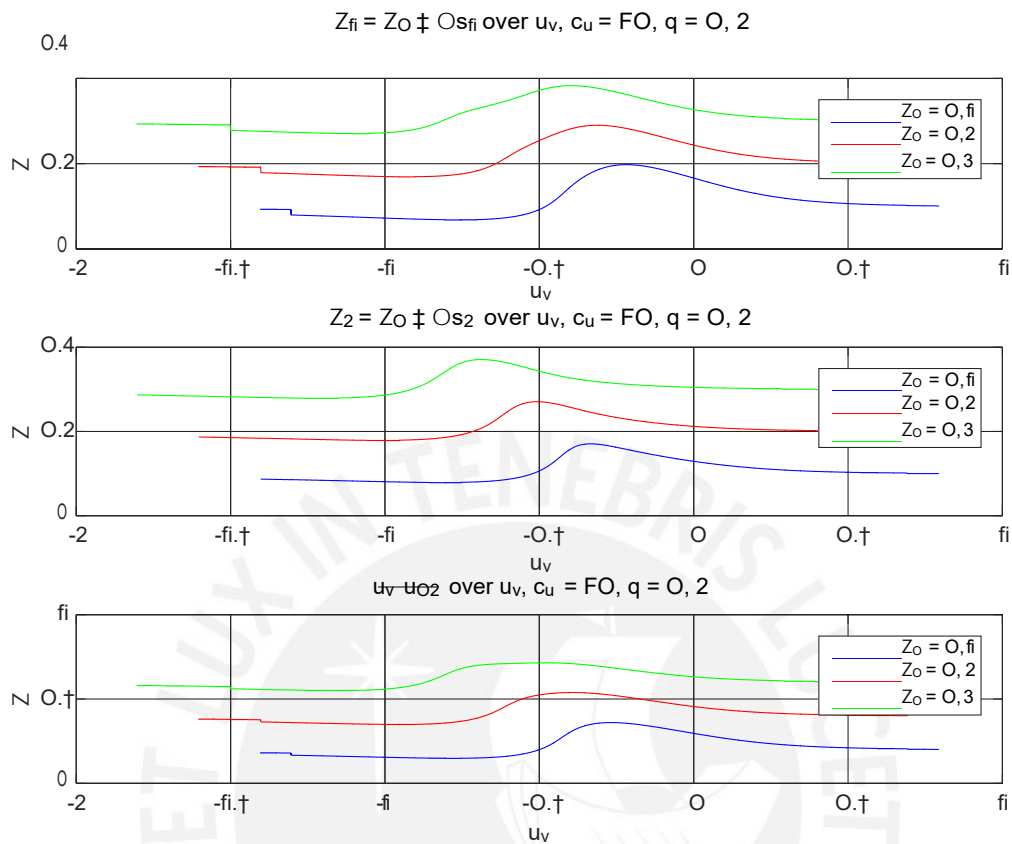


Figure 6.24: Spring lengths λ_i over x_i for model FBFBR, with varied relaxed length of the spring λ_0 .

In all models a variation of the parameters spring stiffness, relaxed spring length and object distance leads to three different effects:

Shifting the signals on the x axis:

A change of the spring properties (spring stiffness c_x and relaxed spring length λ_0) leads to a shift of the support reactions and spring lengths above x_r . Thus a reduction of the spring stiffness c_x and an increase of the relaxed spring length leads to a shift in the negative x_r direction.

While a variation of the spring stiffness c_x only leads to a shift of the maximum values, a variation of the relaxed spring length results in an offset of the whole signal.

Changing the signal width:

Also the signal width depends on the spring stiffness c_x . This parameter is used to implement the coupling between the two beams. A reduction of the spring stiffness leads to narrower signals in the support reactions. The effect of the signal width change when the spring

properties are varied is most evident in the FBFB model. The additional feedback in model FBFBR reduces this.

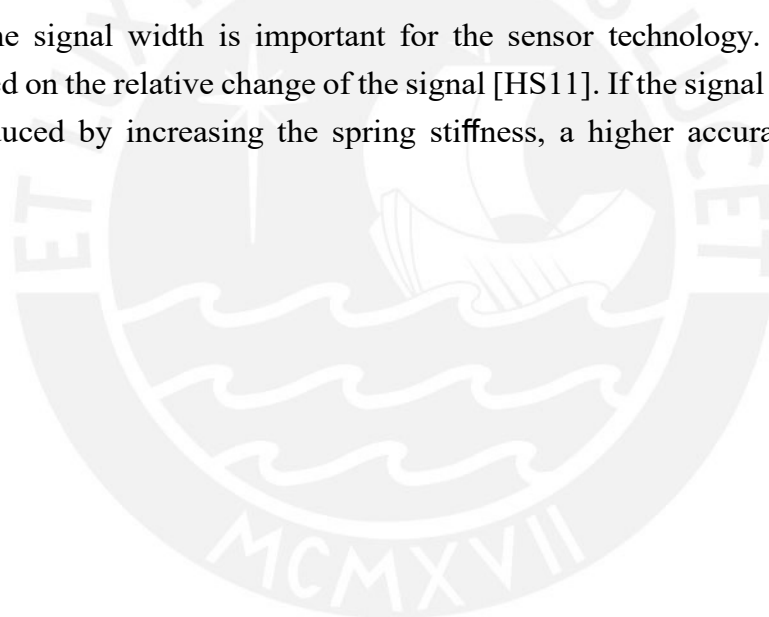
Change of the maximum values:

A change of the maximum values only occurs when the object distance q is changed. Thus, a reduction of the distance leads to an increase in the maximum values of the support reactions.

The comparison of the models of two beams with and without feedback (model FBFB and model FBFBR) shows that the additional spring means that the effects mentioned are less pronounced.

There are also advantages with regard to the reconstruction of the object. The position of the vertex of the object can be determined on the basis of the position of the manipulated variable at which the type of loading of the spring changes from tension to compression.

Furthermore, the signal width is important for the sensor technology. A large number of sensors are based on the relative change of the signal [HS11]. If the signal width of the support reactions is reduced by increasing the spring stiffness, a higher accuracy of the sensor is obtained.



Conclusions and outlook

The present work contributes to the development of a biologically inspired tactile sensor system. Based on the model of special tactile hairs (vibrissae) from the animal kingdom, a mechanical model is to be developed and investigated, taking into account the elastic support and coupling of vibrissae.

An analysis of the current state of scientific knowledge about the biology of vibrissae and their properties considered for modelling was carried out in chapter 2. These can be summarized as follows:

- Vibrissae are yielding, elastic feelers and have a long, slender shape. They have no receptors and only act as a stimulus transmitter [Kla99].
- Vibrissae are elastically mounted in the follicle-sinus complex. That's where the mechanoreceptors are located [Kla99].
- It is hypothesized that the follicle-sinus-complex allows a controllable elasticity by changing the blood pressure [Car09].
- Vibrissae mostly occur in groups; the distances between the individual hairs are small [Kla99].
- Vibrissae can not only be used actively by activating the muscles, but also passively for scanning objects [Car09].

The literature research carried out in chapter 3 showed that a variety of mechanical models of a tactile sensor for active and passive object sensing exist. However, these are mostly limited to a single, clamped vibrissa. In this context, a research deficit in the field of elastically supported, coupled vibrissae was found. This led to the specification of the task and the objective of the present work formulated in chapter 4. In chapter 5 the existing mechanical model from [Ste13] was extended by an elastic support. The actual vibrissa is modelled as an Euler-Bernoulli beam, the elasticity of the skin and tissue as mechanical spring elements. Within the scope of the modelling, the support and coupling of the individual vibrissae was considered at different levels of abstraction. These differ in the number and arrangement of the spring elements:

- Model FB: a beam with an upstream spring
- Model FBFB: two spring-coupled beams with upstream spring
- Model FBFBR: two spring-coupled beams with upstream spring and feedback

When scanning a strictly convex object, a distinction is made between tip and tangential contact (phase A and phase B) following the example of [Ste13]. Furthermore, in the context of the present work, a distinction had to be made for the models with several vibrissae / beams as to which beams are in contact with the object. Based on this, corresponding special cases were derived for the equations for determining the base point position of the individual beams.

In the chapter 5 a verification of the mechanical model and the sampling algorithm implemented in *MATLAB* was performed. For this purpose, the simulation results of the present work were compared with those of a parallel work in which a multi-body model was used.

In chapter 6 parameter studies were carried out for the models described above. The influence of spring stiffness, object distance and relaxed spring length were investigated.

A decrease in spring stiffness and an increase in the relaxed length of the spring will result in a shifting of signals in the negative x direction. Furthermore, a reduction of the spring stiffness leads to a shrinking of the signal width. A changing the maximum values can only be achieved by varying the object distance. The maximum values are thus independent of the spring parameters (spring stiffness and relaxed length).

The results of the present work form the basis for further investigations in the context of elastic vibrissae coupling. During the verification of the simulation models by means of a multi-body model [Mü20], deviations due to dynamic effects occurred at higher scanning speeds. These manifest themselves both in the deformation states of the beam, especially through the impact of the first contact (see fig. 7.1), and in the support reactions (see fig.

7.2). These show a clear noise. In order to consider dynamic effects, the elastic spring model should be adjusted in future work.

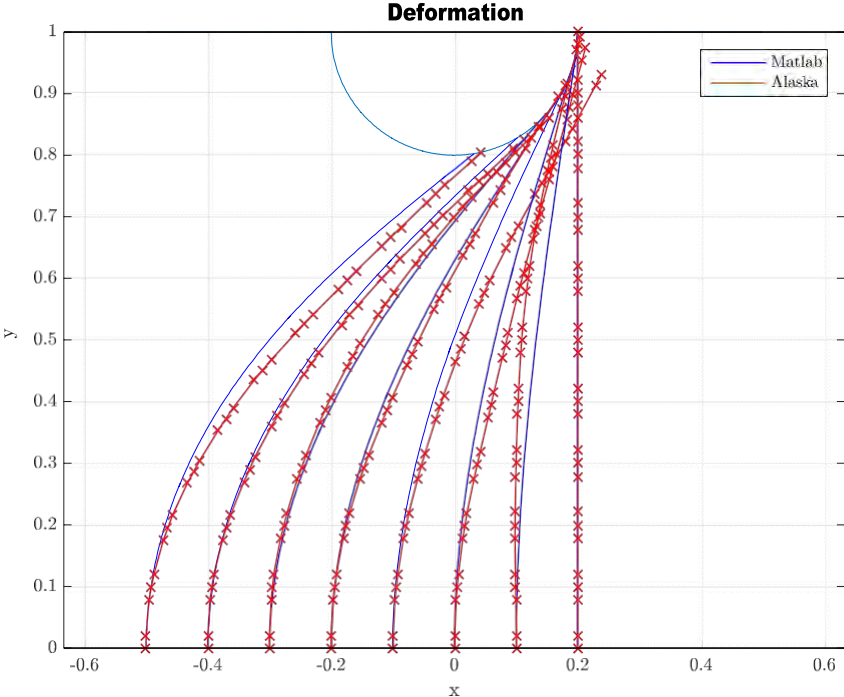


Figure 7.1: Comparison of the deformations of the vibrissae when scanning a cylinder.

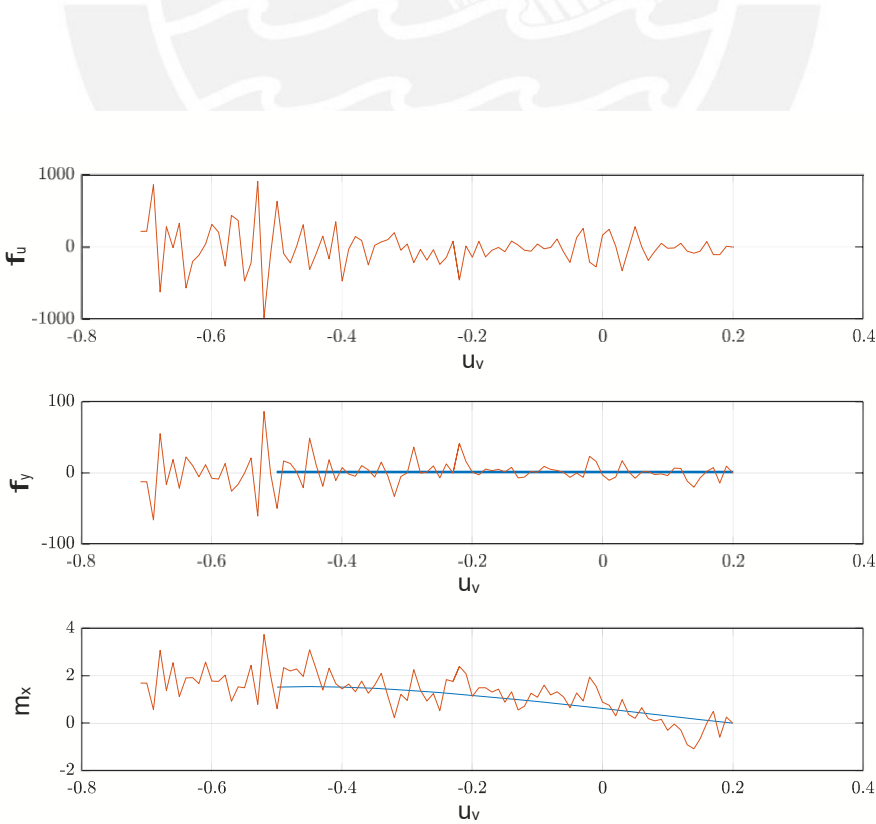


Figure 7.2: Comparison of the support reactions at the vibrissae when scanning a cylinder.

In future work, the possibility of reconstructing the object with the help of the support reactions simulated in this work should be further examined. For this purpose it has to be examined which model parameters (spring stiffness, relaxed spring length and object distance) are required for a reconstruction. It is conceivable that the relaxed length of the spring is necessary for a clear assignment of the base point positions of the beams.

Furthermore, it is conceivable to analyze the influence of a third beam by extending the model as shown in Figure 7.3. For this purpose a recalculation of the foot points must be carried out analogous to section 5.4.3. The following equations result for the general case:

$$\begin{aligned}
 x_{01}'' &= \frac{f_1 - x_{02}c_2 - x_1c_1}{c_1 - c_2} \\
 x_{02}'' &= \frac{f_2 - x_{01}c_2 - x_{03}c_3 - x_1c_4}{c_2 - c_3 - c_4} \\
 x_{03}'' &= \frac{f_3 - x_{02}c_3 - x_1c_5}{c_3 - c_5}
 \end{aligned}
 \tag{7.1}$$

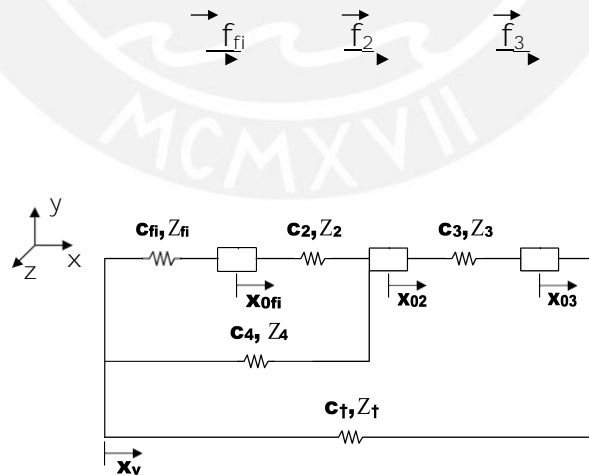


Figure 7.3: Equivalent circuit diagram 3 vibrissae with coupling to the frame.

Subsequently, corresponding special cases can be derived according to the possible contact constellations of the individual beams with the object. The possible scenarios are as follows:

- Flag Phase = 1: only beam 1 in contact
- Flag Phase = 2: only beam 2 in contact
- Flag Phase = 3: only beam 3 in contact
- Flag Phase = 4: beam 1 and 2 in contact
- Flag Phase = 5: beam 2 and 3 in contact
- Flag Phase = 6: beams 1, 2 and 3 in contact

Figure 7.4 shows the support reactions of a pre-simulation. At first, no new effects are visible. However, some parameter studies should also be carried out for this model to confirm the statements.

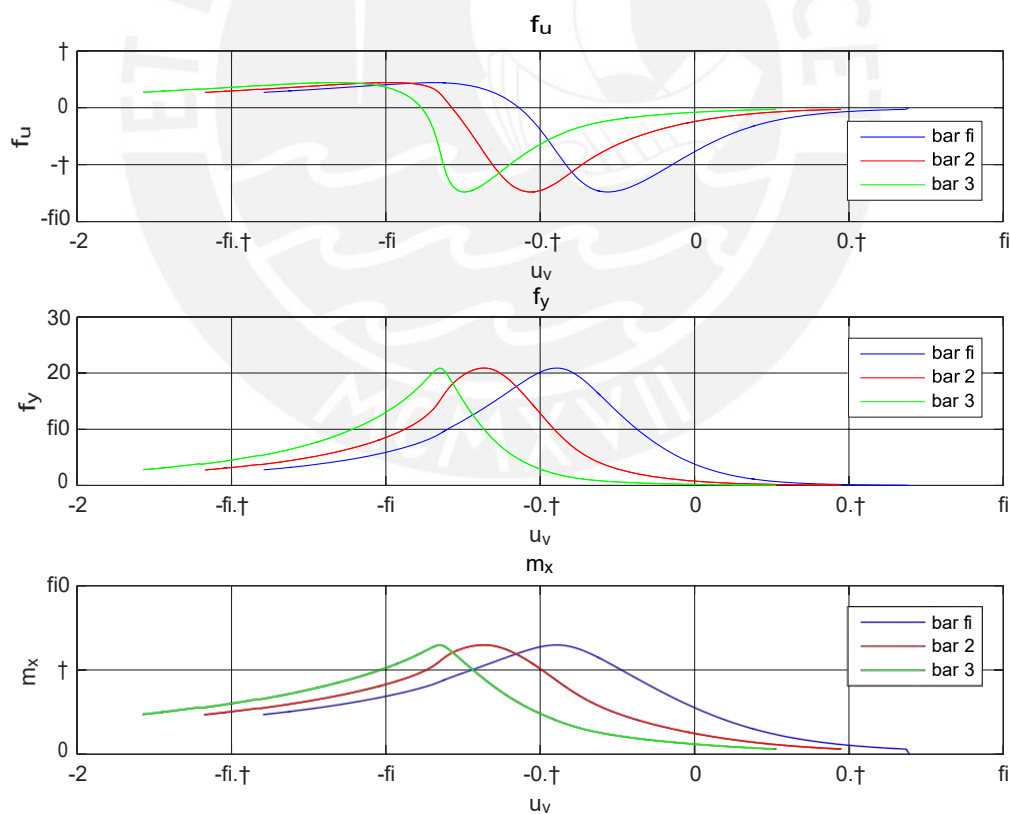


Figure 7.4: Support reactions for the model 3 beam above x_p .

Since vibrissae are elastically coupled with each other not only in their end point, an adaptation of the model according to figure 7.5 would be conceivable. However, this would lead to a three-point boundary value problem and to a tilting of the spring in case of large deformations.

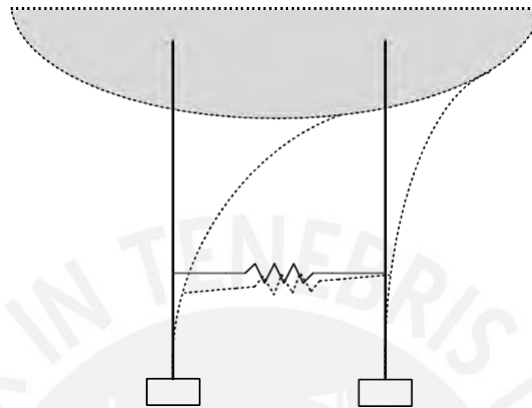


Figure 7.5: Change of the spring position when the point of application of the spring is above the base point.

In the following, further aspects for future work will be briefly described:

- **Consideration of an elastic support in vertical direction or a torsion spring:** The follicle-sinus-complex offers the vibrissa in nature elasticity in all directions. It remains to be examined what effects an elastic support in vertical direction or a torsion spring has on the signals in the support.
- **Expansion of the model for spatial problems:**
The model used has so far been limited to a flat system. In reality, however, three-dimensional scanning processes are also desirable and necessary [SH08]. For this reason, a model for scanning and reconstruction should be developed taking into account an elastic support.
- **Consideration of friction:**
In the current model for scanning, friction is neglected. In order to detect influences due to this, an extension of the model by considering friction effects in the contact point is useful.
- **Practical implementation:**
For a further verification of the simulation models created, it makes sense to implement the models created in the form of an experimental setup. This allows the determination of the support reactions and spring lengths as well as empirical studies with regard to friction effects.

Bibliography

- [AHD09] E. Arabzadeh, M. Heimendahl, and M. Diamond. Vibrissal texture decoding. *Scholarpedia*, 4(4):6640, 2009. revision #150523.
- [Ahl05] Alwynelle S. Ahl. The role of vibrissae in behavior: A status review. *Veterinary Research Communications*, 10:245–268, 2005.
- [AK11] E. Ahissar and P. M. Knutsen. Vibrissal location coding. *Scholarpedia*, 6(10):6639, 2011. revision #151626.
- [BK03] R. W. Berg and D. Kleinfeld. Rhythmic whisking by rat: retraction as well as protraction of the vibrissae is under active muscular control. *Journal of Neurophysiology*, 89 1:104–117, 2003.
- [BPM97] M. Brecht, B. Preilowski, and M. M. Merzenich. Functional architecture of the mystacial vibrissae. *Behavioural brain research*, 84(1-2):81–97, 1997.
- [Car09] K. Carl. Technische biologie des tasthaar-sinnessystems als gestaltungsgrundlage für taktile stiftführende mechanosensoren. Dissertation, Technische Universität Ilmenau, 2009.
- [CK06] J. Curtis and D. Kleinfeld. Seeing what the mouse sees with its vibrissae: A matter of behavioral state. *Neuron*, 50:524–526, 2006.
- [CR06] T.N. Clements and C. Rahn. Tree-dimensional contact imaging with an actuated whisker. *IEEE Transactions on Robotics*, 22(4), 08/2006.
- [Dö82] J. Dörfl. The musculature of the mystacial vibrissae of the white mouse. *Journal of anatomy*, 135(1):147–154, 1982.

- [EKM⁰²] S. Ebara, K. Kumamoto, T. Matsuura, J. Mazurkiewicz, and F. Rice. Similarities and differences in the innervation of mystacial vibrissal follicle-sinus complexes in the rat and cat: A confocal microscopic study. *The Journal of comparative neurology*, 449:103–19, 2002.
- [FPR97] B. Fundin, K. Pfaller, and F. Rice. Different distributions of the sensory and autonomic innervation among the microvasculature of the rat mystacial pad. *The Journal of Comparative Neurology*, 389(4):545–568, 1997.
- [GHSW17] D. Gross, W. Hauger, J. Schröder, and W.A. Wall. *Technische Mechanik 2 Elastostatik*. Springer Vieweg, 13 edition, 2017.
- [HPSG13] S. A. Hires, L. Pammer, K. Svoboda, and D. Golomb. Tapered whiskers are required for active tactile sensation. *eLife*, 2, 2013.
- [HS11] S. Hesse and G. Schnell. *Sensoren für die Prozess- und Fabrikautomation*. Vieweg+Teubner, 5 edition, 2011.
- [HVN¹⁴] T. Helbig, D. Voges, S. Niederschuh, M. Schmidt, and H. Witte. The mechanics of carpal vibrissae of *rattus norvegicus* during substrate contact. *Shaping the Future by Engineering: Proceedings ; 58th IWK, Ilmenau Scientific Colloquium, Technische Universität Ilmenau, Germany, 8-12 September 2014*, 58, 2014.
- [IW75] L. Ibrahim and E.A. Wright. The growth of rats and mice vibrissae under normal and some abnormal conditions. *Journal of Embryology and Experimental Morphology*, 33(4):831–844, 1975.
- [Kla99] G. J. Klauer. *Vibrissen analyse eines taktilen sinnesorgans band 1*. Habilitation thesis, Universität Gesamthochschule Essen, 1999.
- [Kre10] M. Krehbiehl. *Anatomie der rostralen und caudalen tasthaare beim sambischen riesengraumull (*fukomys mechowii*) - sinushaare oder leithaare?* Dissertation, Tierärztliche Hochschule Hannover, 2010.
- [LN99] M. Lee and H. Nicholls. Tactile sensing for mechatronics — a state of the art survey. *Mechatronics*, 9:1–31, 1999.
- [MBSZ19] L. Merker, C. Behn, J. Steigenberger, and K. Zimmermann. Vibrissa-based sensor models with compliant support for object detection. *12th HSTAM International Congress on Mechanics Thessaloniki, Greece, 22 – 25 September 2019*, 2019.
- [Mer17] L. Merker. *Objektabtastung und -konturerkennung durch rotatorisch gelagerte, taktile sensoren mittels nichtlinearer balkentheorie*. Masterarbeit, Technische Universität Ilmenau, 2017.

- [MFS⁺20] L. Merker, C. S. J. Fischer, M. Scharff, M. J. H. Alencastre, and C. Behn. Effectsofmulti-pointcontactsduringobjectcontoursscanningusingabiologically-inspired tactile sensor. *Sensors*, 20(7), 2020.
- [MGA⁺11] B. Mitchinson, R. Grant, K. Arkley, V. Rankov, I. Perkon, and T. Prescott. Active vibrissal sensing in rodents and marsupials. *Philosophical transactions of the Royal Society of London. Series B, Biological sciences*, 366(1581):3037–3048, 2011.
- [MSZB18] L. Merker, M. Scharff, K. Zimmermann, and C. Behn. Signal tuning of observables at the support of a vibrissa-like tactile sensor in different scanning scenarios. In *Proceedings of the 7th IEEE International Conference on Biomedical Robotics and Biomechanics (Biorob), Enschede, Netherlands, 26-29 August 2018*, pages 1138–1143, 2018.
- [Mü20] S. Müller. Determination of the signals recorded by carpal vibrissae of rats during locomotion and forelimb touch down. Master thesis, Technische Universität Ilmenau, 2020.
- [Pea62] O. P. Pearson. Survival value of vibrissae. In *Journal of Mammalogy*, volume 43, page 105, 1962.
- [PMG11] T. J. Prescott, B. Mitchinson, and R. A. Grant. Vibrissal behavior and function. *Scholarpedia*, 6(10):6642, 2011. revision #189995.
- [QH12] B. Quist and M. Hartmann. Mechanical signals at the base of a rat vibrissa: the effect of intrinsic vibrissa curvature and implications for tactile exploration. *Journal of Neurophysiology*, 107(9):2298–2312, 2012.
- [SBH⁺10] E. Simony, K. Bagdasarian, L. J. Herfst, M. Brecht, E. Ahissar, and D. Golomb. Temporal and spatial characteristics of vibrissa responses to motor commands. *The Journal of Neuroscience*, 30(26):8935–8952, 2010.
- [SH08] J. Solomon and M. Hartmann. Artificial whiskers suitable for array implementation: Accounting for lateral slip and surface friction. *Robotics, IEEE Transactions on*, 24(5):1157 – 1167, 2008.
- [SSWB11] M. Schaefer, T. Schmitz, C. Will, and C. Behn. Transversal vibrations of beams with boundary damping in the context of animal vibrissae. *56th International scientific colloquium, Technische Universität Ilmenau, Germany, 12–16 September 2011*, 2011.

- [Ste13] J. Steigenberger. A continuum model of passive vibrissae. *Preprint / Technische Universität Ilmenau, Institut für Mathematik*, 2013.
- [SWZ⁺14] M. Schmidt, H. Witte, K. Zimmermann, S. Niederschuh, T. Helbig, D. Voges, I. Husung, T. Volkova, C. Will, C. Behn, J. Steigenberger, and G. J. Klauer. Technical, non-visual characterization of substrate contact using carpal vibrissae as a biological model: an overview. *58th Ilmenau scientific colloquium, Technische Universität Ilmenau, Germany, 08–12 September 2014*, 2014.
- [TQG⁺11] R. Towal, B. Quist, V. Gopal, J. Solomon, and M. Hartmann. The morphology of the rat vibrissal array: A model for quantifying spatiotemporal patterns of whisker-object contact. *PLoS Computational Biology*, 7(4), 2011.
- [TSJH12] C. Tuna, J. H. Solomon, D. L. Jones, and M. J. Z. Hartmann. Object shape recognition with artificial whiskers using tomographic reconstruction. *International Conference on Acoustics, Speech, and Signal Processing, ICASSP, Kyoto, Japan, 25-30 März 2012*, pages 2537–2540, 03 2012.
- [VCK⁺12] D. Voges, K. Carl, G. J. Klauer, R. Uhlig, C. Schilling, C. Behn, and H. Witte. Structural characterization of the whisker system of the rat. *Sensors Journal, IEEE*, pages 332–339, 2012.
- [WBS17] C. Will, C. Behn, and J. Steigenberger. Object contour scanning using elastically supported technical vibrissae. *ZAMM · Z. Angew. Math. Mech.* 1–17, 2017.
- [Wel18] B. Welsch. Feine antennen. *Info* 47, 06/2018.
- [WK10] C. Williams and E. Kramer. The advantages of a tapered whisker. *PLoS ONE*, 5(1), 2010.

Support reactions for directional and angular forces

F_N = Numeric calculation

F_{MKS} = Multi-body system calculation

Table A.1: Angular force amplitude variation.

Angular force amplitude varies	Fx	Fy	Mz
N: $F = 1$	0.8795	0.4758	0.9755
MKS: $F = 1$	0.9311	0.5075	1.0279
N: $F = 3$	0.5139	2.9557	2.4313
MKS: $F = 3$	0.5295	3.0606	2.5185
N: $F = 5$	-2.5163	4.3207	2.9396
MKS: $F = 5$	-2.6064	4.4662	3.0413
N: $F = 7$	-5.9366	3.7091	2.7236
MKS: $F = 7$	-6.0587	3.8178	2.8300
N: $F = 10$	-9.8894	1.4833	1.7224
MKS: $F = 10$	-9.9876	1.4674	1.8232

Table A.2: Angular force application point variation.

Angular force application point varies:	F _x	F _y	M _z
N: S1 “ 30%	0.9990	0.0450	0.2999
MKS: S1 “ 30%	1.0384	0.0477	0.3134
N: S1 “ 50%	0.9922	0.1246	0.4992
MKS: S1 “ 50%	1.0367	0.1320	0.5238
N: S1 “ 70%	0.9703	0.2421	0.6958
MKS: S1 “ 70%	1.0194	0.2593	0.7321
N: S1 “ 100%	0.8795	0.4758	0.9755
MKS: S1 “ 100%	0.9311	0.5075	1.0279

Table A.3: Directional scatter force amplitude variation.

Directional scatter force amplitude varies:	F _x	F _y	M _z
N: F “ 1	1	0	0.9437
MKS: F “ 1	1.0472	0.0035	0.9851
N: F “ 3	3	0	2.2367
MKS: F “ 3	3.1103	0.0026	2.3183
N: F “ 5	5	0	3.0619
MKS: F “ 5	5.2385	0.0674	3.2040
N: F “ 7	7	0	3.6895
MKS: F “ 7	7.2107	0.0477	3.8007
N: F “ 10	10	0	4.4500
MKS: F “ 10	10.3494	0.0190	4.6039

Table A.4: Directional force application point Variation.

Directional scatter force application point varies:	F _x	F _y	M _z
N: S1 “ 30%	1	0	0.2998
MKS: S1 “ 30%	1.0395	0.0005	0.3133
N: S1 “ 50%	1	0	0.4979
MKS: S1 “ 50%	1.0448	0.0006	0.5223
N: S1 “ 70%	1	0	0.6893
MKS: S1 “ 70%	1.0498	0.0041	0.7239
N: S1 “ 100%	1	0	0.9436
MKS: S1 “ 100%	1.0472	0.0035	0.9851